UNIVERSITY OF CALIFORNIA,
IRVINE

3D-printed, wireless, and battery-free wearable sensor systems for on-demand personal health monitoring

DISSERTATION

submitted in partial satisfaction of the requirements
for the degree of

MASTER OF SCIENCE

in Electrical Engineering

by

Sahar Najafikhoshnoo

Thesis Committee:
Assistant Professor Rahim Esfandyarpour, Chair
Assistant Professor Quinton Smith
Assistant Professor Hamidreza Aghasi

2023

DEDICATION

This dissertation is warmly dedicated to the key figures in my life who have provided me with endless support, inspiration, and encouragement.

First and foremost, to my dear parents, Farahnaz and Hamzeh, who have always been my source of strength and inspiration. You have instilled in me the passion for learning, the courage to persist, and the determination to excel. Your unconditional love, ceaseless support, and unwavering faith in me have paved the way for this achievement.

To my sister, Setareh, your camaraderie, your belief in my abilities, and your constant encouragement have been the pillars of my strength in this journey. I'm forever grateful for having a sister like you.

To my fiancé, Arvin, my partner in every sense, your love, patience, and understanding have been my refuge during this arduous process. Your unwavering support and faith in me, even in the darkest of times, have been a shining beacon that has guided me towards this accomplishment.

Every page of this dissertation carries a piece of you all, an imprint of your influence, love, and belief. Thank you for making this journey not just possible, but meaningful and unforgettable. This achievement is as much yours as it is mine.

Table of Contents

LIST OF PAPERS

Chapter 2 is largely based on the following papers:

- Yi, Q., Najafikhoshnoo, S., Das, P., Noh, S., Hoang, E., Kim, T., & Esfandyarpour, R. (2022). All-3D-Printed, Flexible, and Hybrid Wearable Bioelectronic Tactile Sensors Using Biocompatible Nanocomposites for Health Monitoring. Advanced Materials Technologies, 7(5), 2101034.

Chapter 3 is largely based on the following papers:

- NajafiKhoshnoo, S., Kim, T., Tavares-Negrete, J. A., Pei, X., Das, P., Lee, S. W., Rajendran, J., & Esfandyarpour, R. (2023). A 3D Nanomaterials-Printed Wearable, Battery-Free, Biocompatible, Flexible, and Wireless pH Sensor System for Real-Time Health Monitoring. Advanced Materials Technologies, 8(8), 2201655.
- Najafikhoshnoo, Sahar, and Rahim Esfandyarpour. "3D-printed, wireless, and battery-free wearable sensor system for on-demand personal health monitoring (Conference Presentation)." Biophotonics in Exercise Science, Sports Medicine, Health Monitoring Technologies, and Wearables IV. SPIE, 2023.

LIST OF FIGURES

Page

LIST OF ABBREVIATIONS

Variable name	Description
CNT	Carbon Nano Tube
PDMS	Polydimethylsiloxane
SEM	Scanning Electron Microscopy
PVA	Poly Vinyl Alcohol
WE	Working Electrode
RE	Reference Electrode
NFC	Near Field Communication
SEBS	Styrene-Ethylene-Butylene-Styrene
PANI	Polyaniline
PI	Polyimide
ADC	Analog-to-Digital Converter

ACKNOWLEDGMENTS

I would like to express my deepest gratitude and appreciation to the committee chair, Prof. Rahim Esfandyarpour, who constantly motivated me to innovate and strived to bring out the best in me. Without his support, guidance, and persistent help, this thesis would not have been possible. During my term in his lab, I have learned many aspects of scientific research which will undoubtedly be invaluable in my future career.

I have the deepest gratitude for my committee members, Prof. Hamidreza Aghasi, and Prof. Quinton Smith for their invaluable feedback on my thesis. I would also like to thank my colleagues in Integrated Nano Bio Electronics Innovation (INBE) laboratory, in particular Dr. Prativa Das, and Dr. Taeil Kim, and other PhD students, Jorge Tavares-Negrete, and Xiaochang Pei for providing valuable research advice and helping me troubleshoot problems encountered during experiments.

I would like to thank UCI's Department of Electrical Engineering and Computer Science, for giving me the initial fellowship funding which enabled me to thrive in this wonderful path.

ABSTRACT OF THE THESIS

3D-printed, flexible, wireless, and battery-free wearable sensor systems for on-demand personal health monitoring

by

Sahar Najafikhoshnoo

Master of Science in Electrical Engineering

University of California, Irvine, 2023

Assistant Professor Rahim Esfandyarpour, Chair

Wearable sensors and electronics have emerged as integral components of personalized healthcare, playing an instrumental role in real-time monitoring of critical physiological parameters. These devices provide pivotal information about an individual's health status, effectively revolutionizing medical assessment and intervention procedures. The role of wearable sensors extends across a diverse range of healthcare applications, from early disease diagnosis and tracking of chronic conditions, to the real-time evaluation of treatment efficacy. In response to these growing needs, this thesis seeks to confront the prevailing challenges in healthcare monitoring through the design, development, and comprehensive characterization of innovative sensor systems. These systems leverage novel multi-material and multilayer 3D printing technology to expedite and streamline the production of various wearable sensing devices. The simplicity of these manufacturing

processes enables individuals with basic computer and 3D printing knowledge to execute them without necessitating cleanroom micro-nanofabrication facilities. As a result, these cost-effective platforms, with their straightforward and cleanroom-free manufacturing, have the potential to transform personalized healthcare significantly.

Chapter 2 delves into the design, fabrication, and experimental findings of an all-3D-printed, multi-material, multilayer nanocomposite-based (M2A3DNC) flexible wearable pressure sensor. This sensor system is remarkable for its high sensitivity, rapid response time, and extraordinarily low detection limit, making it perfectly suited for recording multiple, sensitive physiological signals in real-time.

Chapter 3 elucidates the development and experimental results of a wireless, battery-free, biocompatible, flexible 3D-printed (W2BF3D) wearable pH sensor with an integrated near-field communication (NFC) readout system. This system exhibits high sensitivity, specificity, repeatability, and reproducibility across various pH ranges and allows for real-time, in-situ sweat pH monitoring.

Our proposed manufacturing methodology for sensor systems offers a promising shift in the realm of healthcare monitoring technologies. We envision that our easily fabricable, user-friendly, scalable, and low-cost sensor systems will emerge as potential game-changers in personalized healthcare, catalyzing a significant transformation in health monitoring practices.

Chapter 1

Introduction

This chapter introduces the specific research problems addressed in this work by explaining the organization and content of this thesis in detail. Section 1.1 offers a concise overview of the research issue addressed in this work. Section 1.2 elucidates the layout and substance of the thesis, complemented by a summarization of the findings on a chapter-by-chapter basis.

1.1 Introduction to the research problem

Wearable sensors and electronics have become an essential component of personalized healthcare, enabling real-time monitoring of vital physiological signals and providing crucial information about a person's health. The transformative power of these devices lies in their ability to provide a dynamic view of individual health, augmenting the traditional snapshot approach that has long dominated healthcare. Wearable sensors have catalyzed a significant shift in the healthcare landscape by offering an innovative mechanism for early detection and continual tracking of disease state, They have not only made it possible to monitor health conditions in real time but have also fostered the development of treatment strategies that are responsive to the dynamic nature of our physiological states.

To date, a plethora of biosensors have been developed with the capacity to detect a diverse range of physiological signals and biological biomarkers. Physiological sensors, designed to monitor vital signs, have been crucial in this evolution. They are capable of

tracking key physiological parameters such as heart rate, blood pressure, oxygen saturation, and body temperature, amongst others. Heart rate sensors, for instance, are now a ubiquitous component of fitness trackers and smartwatches, furnishing real-time insights about cardiovascular health and fitness levels. Blood pressure sensors, integrated into select wearables, allow for continuous monitoring, an essential for managing conditions like hypertension. Pulse oximeters, measuring oxygen saturation in the blood, have gained particular relevance in monitoring respiratory conditions, especially during the COVID-19 pandemic.

In parallel, biological biomarker-detection sensors are making waves in healthcare technology. They can quantify a wide array of biomarkers such as lactate, glucose, pH levels, and human chorionic gonadotropin hormone, providing vital insights into various health conditions. Lactate, for example, is a crucial indicator of tissue oxygenation and is vital in the management of critical care patients. Continuous monitoring of glucose levels is paramount in diabetes management. Moreover, pH levels can reflect various body functions and can be especially useful in diagnosing gastrointestinal disorders, while the human chorionic gonadotropin hormone is a valuable biomarker in both pregnancy testing and in the diagnosis of certain types of cancer.

Over the years, various wearable sensors have been fabricated using 2D planar processes[1], such as photolithography[2], laser writing[3], and metal deposition[4]. However, most of these methods have suffered from issues arising from complicated manufacturing processes, high fabrication costs, and uncontrollability, which seriously restricts the development of the wearable sensors.[1], [4], [5] The recent advancements in the development of different conducting inks (e.g., nanoparticles, nanotube compositions), and insulating inks (i.e., polydimethylsiloxane (PDMS), styrene-ethylene-butylene-styrene

(SEBS)) in combination with rapid 3D-printing technology, have enabled us to manufacture various wearable sensing devices more rapidly and cost-effectively.[6]

This thesis aims to address the challenges described above by developing and fully characterizing novel, ultra-low cost, easy to manufacture, sensory systems with high sensitivity, very good specificity, repeatability, and reproducibility for healthcare monitoring by incorporating novel multi-material and multilayer 3D printing to manufacture various wearable sensing devices more rapidly and cost-effectively. The manufacturing process of these platforms is extremely simple and straightforward without the need for cleanroom micro-nanofabrication facilities. Due to their low-cost and simple, straightforward, and cleanroom-free manufacturing process, these platforms could potentially revolutionize personalized healthcare. Chapter 2 of this thesis presents the design, fabrication and experimental results of our all-3D-printed pressure sensor. Chapter 3 of this thesis presents the design, fabrication, and experimental results of our 3D-printed, flexible and wireless pH sensor system. More details on the organization and content of this thesis can be found in the next section.

1.2 Organization and content

This thesis comprises two main chapters (chapters 2 and 3), each presenting a distinct research project. These chapters can be read independently. Each chapter begins with an 'introduction' that emphasizes the specific problem, its scientific and practical importance, and includes an overview of relevant literature. Certain terms are shortened for simplicity and are explained upon their first use. Following the introduction, the 'results' section shares crucial experimental outcomes. This is succeeded by a 'discussion' that deliberates the importance and significance of the results and the potential for future

research. Next, the 'Materials and Methods' section details the experimental process. Key results from chapters 2 and 3 are summarized in the subsequent paragraphs.

Chapter 2: **Fully-3D-Printed, Flexible, and Hybrid Wearable Bioelectronic Pressure Sensors for Health Monitoring.**

In this chapter, we introduce a novel, all-3D-printed, multi-material, multilayer nanocomposite-based (M2A3DNC) flexible wearable pressure sensor. This sensor is designed for recording multiple, sensitive physiological signals in real-time, offering an innovative solution for comprehensive health monitoring. The proposed manufacturing technique enables the rapid and cost-effective development of a highly compressible micro-engineered device, all via a single tool, employing a consecutive multilayer printing approach. Most conventional pressure sensors containing a microengineered active layer are either been fabricated by complicated, expensive, and lengthy microfabrication steps in cleanrooms or by mold-casting techniques.[7] These complicated processes hinder rapid innovation and the broad selection of functional materials alongside with their use in resource-poor regions. To address this challenge, we present a low-cost, simple, and straight-forward fabrication method for pressure sensor leveraging the inherent property of extrusion printing, enabling multilayer and multi-material deposition in a tailorable design.

We demonstrate the design and development of an all-3D-printed nanocomposite-based (M2A3DNC) microengineered flexible wearable pressure sensor for recording sensitive and multiple physiological signals for real-time human health monitoring. Our multilayer 3D-printed sensors demonstrate impressive sensitivity at 0.512 kPa^{-1}, a response time of 94.6 ms, and a low detection limit of <0.009 kPa. These findings underscore the exceptional potential of this multilayer and multi-material 3D printing approach for

structure engineering. This technique has countless potential applications in real-time human health monitoring.

Chapter 3: A 3D-printed, Wireless, Battery-free, and Wearable pH Sensor System for On-demand Personal Health Monitoring.

We introduce a wireless, battery-free, biocompatible, flexible 3D-printed (W2BF3D) wearable pH sensing system featuring a near-field communication (NFC) readout, aiming to resolve prevalent issues in pH monitoring. This system comprises of a disposable pH sensor and a reusable NFC readout system for real-time, in-situ sweat pH monitoring. Fabrication of the W2BF3D pH sensor and NFC circuit occurs on a styrene-ethylene-butylene-styrene (SEBS) substrate and polyimide film respectively for flexibility. SEBS offers human skin-like mechanical traits with excellent flexibility and stretchability up to 300%, closely matching human skin's Young's modulus. The sensor, NFC electronic circuit, and NFC antenna are prepared via multilayer and multi-material 3D printing approach.

The NFC readout system pairs with the W2BF3D pH sensor for wireless, battery-free operation, permitting continuous in-situ monitoring by transmitting measurements to a connected smartphone. These measurements can be logged and displayed on a custom-designed app through the smartphone's NFC module, utilizing the ubiquity of smartphones to advance personalized healthcare by providing wearable, portable systems for continuous data acquisition. This system could promote effective personal healthcare monitoring in homes or even low-resource settings, given its small size, low cost, and user-friendliness.

The W2BF3D wearable pH sensor exhibits high sensitivity, specificity, repeatability, and reproducibility across various pH ranges (5.5 - 7.0), maintaining mechanical stability and flexibility. Bending tests have validated its mechanical flexibility up to 500 cycles, and it showcases high sensitivity near the Nernstian sensitivity (≈−51.76 ± 0.97 mV/pH) and a

correlation coefficient (R^2) of 0.997. Biocompatibility tests confirm its safety for long-term skin contact, achieving 90% cell survivability over five days of culture on the W2BF3D pH sensor. Furthermore, successful ex-situ and in-situ measurements of pH values in artificial and actual sweat are obtained, indicating that the W2BF3D wearable sensing system could provide an integrated platform for accurate, wireless, non-invasive real-time healthcare monitoring with simplicity and cost-efficiency.

Chapter 2

ALL-3D-printed, Flexible, Low-Cost, and Wearable Pressure Sensor for Health Monitoring

2.1 Introduction

Wearable biosensors have become a topic of substantial interest and urgency over the past decade due to their wide-ranging potential applications. These areas include personalized healthcare, electronic skin and textiles, soft robotics, human/machine interfaces, and drug delivery.[8], [9] As we delve deeper into the realm of personalized healthcare, flexible wearable pressure sensors capable of intimate skin contact have gained considerable attention. The ability of these sensors to continuously monitor physiological health signals like wrist pulse, blood pressure, heart rate, and respiration rate has been shown to be instrumental in the early diagnosis of diseases. [10] The working principle of pressure sensors is simple yet effective; they detect the force exerted by a gas or liquid and then convert it into a quantifiable measurement. This process of data collection and conversion allows the device to monitor physiological health signals in real time. Studies have started to corroborate the value of these sensors in disease prediction and prevention. One research established a connection between the human respiratory rate and the risk of infection with the Coronavirus disease (COVID-19), successfully identifying pre-symptomatic individuals with a high degree of accuracy.[11] Similarly, early detection of

unusual systolic blood pressure can potentially mitigate the risk of arterial wall stress and prevent the development of atherosclerosis.

Over the years, the technological evolution in pressure sensors has led to the creation of various classes such as capacitive, resistive/piezoresistive, piezoelectric, and triboelectric sensors.[12] All these have found their niche in healthcare applications. Among these, capacitive-based pressure sensors stand out due to their high sensitivity, low power consumption, simplified design, high flexibility, better resistance to environmental noises, and quick response time to external stimuli.[13]–[16] However to improve the engineered design aspects, it is essential to understand why these characteristics matter in tracking vital signals. High sensitivity, for instance, ensures accurate detection of even the smallest changes in pressure, which is critical for tracking subtle fluctuations in physiological signals. Low power consumption is crucial for long-term monitoring applications where a constant power supply may not be available. High flexibility is important for wearable sensors as they need to conform to the complex contours of the human body. Additionally, fast response time ensures that changes in pressure are detected and reported without delay, enabling real-time monitoring of health signals. Design parameters that contribute to these features include the choice of materials, the design of the electrode and dielectric layers, and the micro-architecture of the sensor. High performance of capacitive pressure sensors makes them highly suitable for monitoring critical human signals, thereby aiding in real-time personalized medicine.

Traditionally, pressure sensors were manufactured using cleanroom-based microfabrication techniques. This process involves a series of complex steps such as photolithography, etching, deposition, and others, which are carried out in a highly controlled environment to avoid contamination.[7] While these methods allow high

precision, they are also time-consuming, costly, and require highly trained personnel.

The rise of additive manufacturing, or 3D printing, offers a more accessible and cost-effective alternative to these conventional methods. Additive manufacturing is a process that creates objects by depositing material layer by layer according to a pre-defined digital model.[17], [18] Unlike traditional fabrication methods that remove material to create a shape, additive manufacturing only uses the material needed to form the object, minimizing waste and allowing for more complex designs. These new methodologies are more convenient, rapid, and cost-effective compared to traditional clean-room-based microfabrication techniques.[19], [20]

One of the significant advantages of 3D printing is its ability to print multi-material, multi-layer structures. This feature is a game-changer for fabricating wearable sensors as it allows for the simultaneous integration of different materials with varied properties into a single device. Moreover, 3D printing provides freedom to adjust the viscosity of the materials used and select from a wide range of materials based on the required application. These capabilities open up new possibilities for the design and fabrication of wearable sensors, enabling the creation of more complex, functional, and efficient devices.

The microengineered active layer is a critical component of pressure sensors that significantly impacts their sensitivity. This layer undergoes deformation when subjected to pressure, leading to a change in the output signal of the sensor. Different micro-engineered designs such as microdomes, micropyramids, lines or microridges, papillae, microspheres, micropores, and microcylinders have been developed to increase the sensitivity and performance of the pressure sensors for specific applications.[21]–[23] By incorporating intricate microstructures within the active layer, the sensor's response to pressure changes can be amplified, leading to improved sensitivity and, consequently, more accurate health

monitoring. To date, most pressure sensors with a microengineered active layer have been created using complicated and time-consuming microfabrication steps in cleanrooms or by mold-casting techniques.[7] These intricate processes have posed significant challenges to rapid innovation and the broad selection of functional materials.

This research work addresses some of the challenges described above by introducing an innovative flexible wearable pressure sensor, fabricated using a pioneering approach involving multi-material and multilayer 3D printing with nanocomposites (M2A3DNC). This sensor is unique in its ability to detect multiple physiological signals with acute sensitivity, paving the way for advancements in real-time health tracking. Our distinctive fabrication process circumvents the need for cleanrooms, instead using multilayer 3D printing in a sequential manner. This approach not only reduces costs but also expedites the fabrication process, resulting in a microengineered device that is highly compressible with high sensitivity and low detection thresholds. We fully characterize and optimize the printing parameters associated with each material and each layer to be able to fully print the pressure sensor. By applying the intrinsic property of extrusion printing, the hemicylinder microstructure dielectric layer was directly 3D printed by managing the moving path of the nozzle, with air voids formation after assembling to enhance the compressibility of the active layer. As a result, our multilayer 3D-printed sensors demonstrated high mechanical tolerance to external distortion, an enhanced high sensitivity as 0.512 kPa^{-1}, a response time of 94.6 ms, and a low detection limit of <0.009 kPa. The device can be used for different signal measurements with an aim to show the potential of our device, not only in real-time human health monitoring but also in robotics tactile sensing and human–machine interfaces.

2.2 Results and Discussion

2.2.1 Design and fabrication of all-3D-printed pressure sensor

The fabrication of the Multi-materials All-3D-Printed Nanocomposites-Based (M2A3DNC) flexible pressure sensors involves a layered approach, utilizing three distinct materials structured in a sequence forming the support layer, conductive material layer, and dielectric layer. A multi-material 3D printing approach using an extrusion-based 3D printer is developed and optimized to achieve the goal, as shown in Figure 2.1a. The extrusion-based 3D printer is adapted for the process, as it can provide automated and digital control of the process. Various designs are constructed layer by layer and printing protocols of different printing materials are optimized to achieve the hybrid structure of the M2A3DNC pressure sensors. To print the support layer of the sensor, first, a blend of two PDMS elastomers, Sylgard 184 and SE 1700, at different ratios are optimized to achieve a printable ink with desired viscosity. Next, to print the conducting layers of the sensors, Carbon Nano Tube (CNT) fillers are mixed with the pure PDMS (Sylgard 184) matrix, to obtain a conductive, biocompatible, and mechanically flexible ink. The conductive layer has been designed to have an island-connected structure to cover a larger area alongside having better mechanical stability. Finally, to fabricate an active micro-structured dielectric layer, Ecoflex 00-30 is utilized due to its biocompatibility, mechanical stability, flexibility, and high mechanical compressibility. The hemicylinder micro-structured dielectric layers are designed and 3D printed by the printer setting of rectilinear infill pattern, and 50 % infill intensity, to have micron-ranged hemicylinder filaments with the pitch gap around 400 μm as shown in Figure 2.1b. Lastly, two parts are assembled, forming air voids in between, to enhance the compressibility of the active layer.

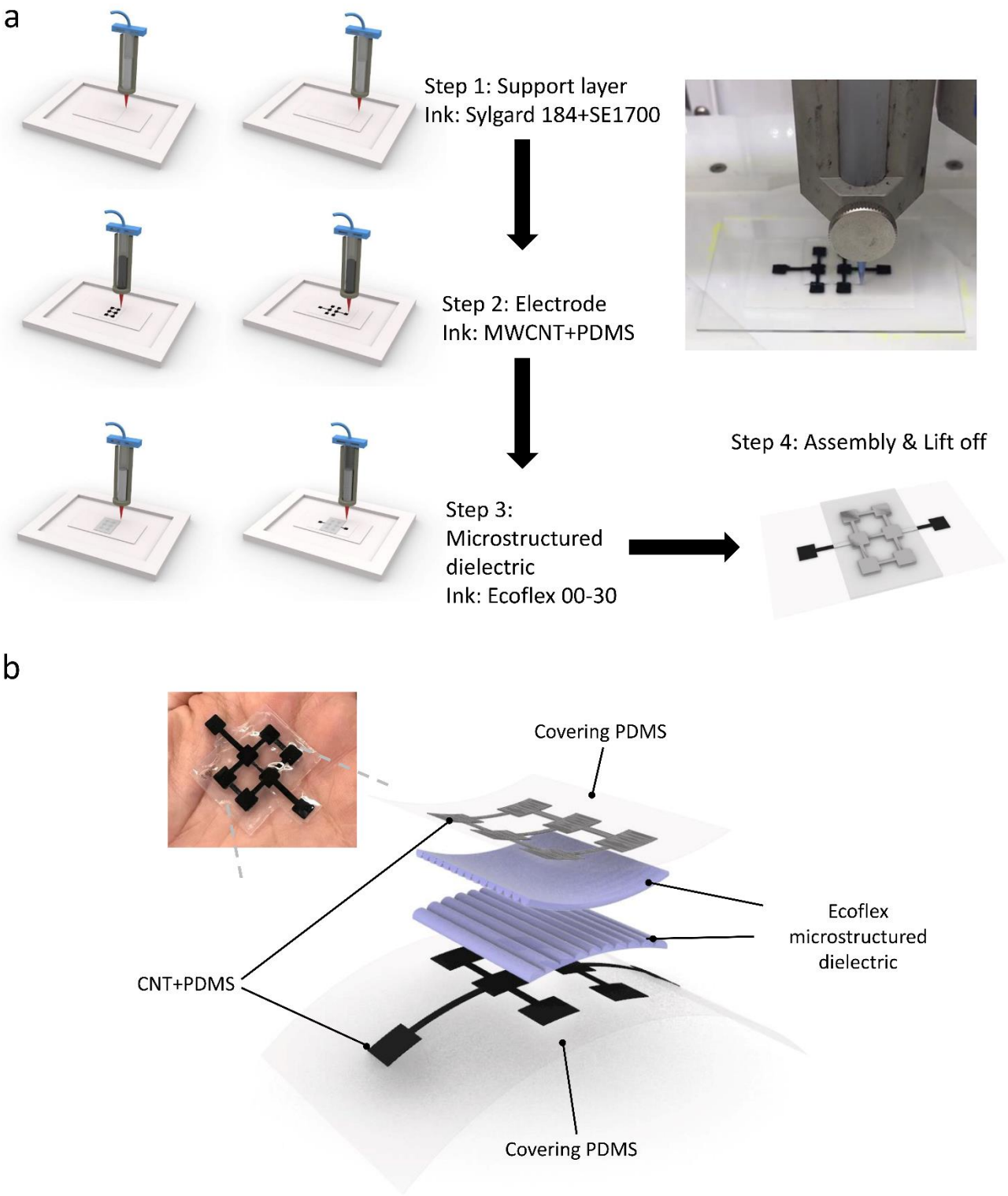

Figure 2.1: **Multi-materials all-3D-printed nanocomposites-based (M2A3DNC) flexible wearable pressure sensors schematic and integration process.** (a) A schematic representation of 3D printing of inks (steps 1-3) to construct a multilayered structure of M2A3DNC sensors followed by its assembly (step 4). Inset: Optical image of 3D printing of hemicylinder patterned Ecoflex dielectric layer. (b) Photograph and the schematic of the exploded view of

the M2A3DNC pressure sensor for multiple physiological signals monitoring.

2.2.2 Printing Parameters Optimization

The construction process utilizes our specifically tailored multi-material 3D printing method, illustrated in Figure 2.1a. Every layer of the M2A3DNC pressure sensors is sequentially crafted through extrusion 3D printing. During this extrusion 3D printing procedure, several print parameters critically impact the precision and quality of the pattern printed, encompassing elements like extrusion pressure control, the speed of the print head movement, and the dimensions of the nozzle. For instance, the rate at which material is extruded relates to the size of the nozzle and the pressure applied, while the deposition is connected to both extrusion and printing speed. If the extrusion speed is low and the printing speed is high, the material is stretched, reducing the width of the line deposited. However, in some scenarios, material deposition can be disrupted. Conversely, with a high extrusion speed and low printing speed, the filament width becomes larger.

To examine the impact of different parameters on resolution and filament features, we conduct characterization experiments. We study the influences of distinct extrusion nozzles (with inner diameters of 510, 340, and 260 μm), the printing speed (ranging from 1 to 7 mm/s), and the extrusion pressure (ranging from 90 to 120 kPa) on the continuity, thickness, width, and electrical resistivity of 3D printed conductive lines (n = 3) using our homemade 12 wt% CNT + PDMS ink (Figure 2.2). Circumstances that can't generate a continuous filament are omitted from the plots, and the standard deviation within the same sample batch is illustrated in error bars (n = 3).

As depicted in Figure 2.2a–f, the precision of the printed features is enhanced by reducing the diameter of the printing nozzle. Using the smallest nozzle with an inner diameter of 0.26 mm, the minimum achievable thickness decreases from 120 to 46 μm by

accelerating the printing speed from 2 to 7 mm/s and decreasing the extrusion pressure from 120 to 90 kPa (Figure 2.2c). Likewise, the minimum attainable width reduces from 407 to 106 μm (Figure 2.2f), and the resistivity drops from 0.114 to 0.019 Ωm (Figure 2.2i). Therefore, the optimized printing conditions are determined to be a printing speed of 7 mm/s, an extrusion pressure of 90 kPa, and an inner nozzle diameter of 0.26 mm, and these parameters are sustained for the printing of the conductive layers during sensor construction.

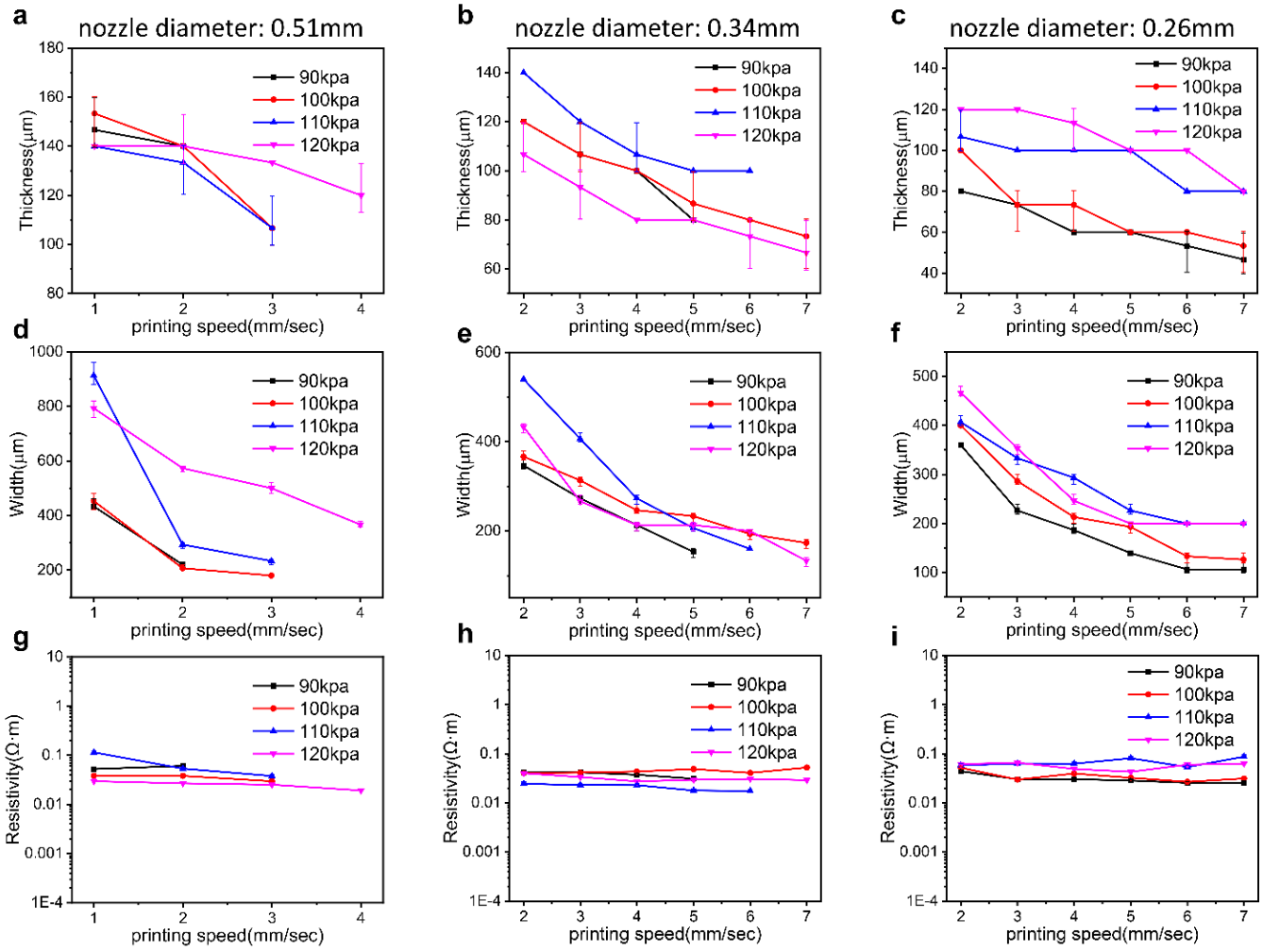

Figure 2.2: Characterization and optimization of 3D bioprinting parameters. (a-c) the thickness of 3D printed conductive lines as a function of printing speed with different printing nozzles at various extrusion pressures, (b) The width of 3D printed conductive lines as a function of printing speed with different printing nozzles at various extrusion pressures,

and (c) The conductivity of 3D printed conductive lines as a function of printing speed with different printing nozzles at various extrusion pressures.

2.2.3 Active Microstructured Dielectric Layer Integration and Sensor Performance

As previously highlighted, amplifying the sensitivity of wearable sensors is pivotal for collecting subtle physiological signals accurately. To accomplish this, we employ a directly 3D printed active microstructured dielectric layer – a porous, grid-shaped patterned dielectric. This layer is designed to enhance the sensor's sensitivity during the consecutive multi-material multilayer printing process. In essence, we configure the printer to produce two hemicylinder-shaped patterned Ecoflex layers using a rectilinear infill pattern, 50% infill intensity, and a speed of 10 mm/s. The final microstructured porous grid-shaped dielectric layer emerges from the assembly of these two perpendicularly printed hemicylinder-structured layers, as depicted in Figure 2.3a.

We scrutinize the 3D printed hemicylinder microstructured dielectric layer using both an optical microscope and scanning electron microscopy (SEM) imaging. The cross-sectional image of a prepared sample for SEM imaging is presented in Figure 2.3c. The layers include i) a hemicylinder-structured dielectric (Ecoflex 00-30 with a peak thickness of approximately 71 μm and pitch thickness of 52 μm, plus a pitch gap of about 400 μm), ii) CNT + PDMS (forming the sensor's conductive layer), and iii) PDMS (forming the sensor's encapsulating layer). These are all 3D printed on double-sided tape attached to a glass substrate, prepping the sample for cross-sectional SEM imaging.

Notably, the Ecoflex layer displays a repeating semicylinder structure when printed directly by the extrusion 3D printing method. An optical microscope image of the Ecoflex dielectric layer, presented in Figure 2.3d, reveals air voids that form between the gaps of the

perpendicularly aligned hemicylinder pattern. This characteristic may enhance the structure's deformation under pressure and thus boost the sensor's sensitivity as desired.

The performance metrics of the M2A3DNC pressure sensors are presently being examined ex situ. In order to ascertain the calibration curve of these sensors, we are quantifying the relative change in capacitance ($\Delta C/C_0$) in correlation with the applied pressure (P), where C_0 designates the baseline capacitance in the absence of any pressure application. The exerted pressure is meticulously regulated with a pressure gauge, and the associated capacitance is documented using an LCR meter.

With regard to the two different configurations of M2A3DNC pressure sensors - those incorporating a micropatterned dielectric layer and those with a planar dielectric layer - five distinct data points are recorded for each pressure load (n = 3) and presented as a mean value complemented with standard deviation (Figure 2.3e). As indicated by the empirical results, the sensitivity, the slope of the calibration curve, of M2A3DNC sensors that employ a microstructured dielectric layer is quantified to be 0.512 kPa^{-1}, approximately 3.2 times higher than that of the sensors with a planar dielectric layer, which has a sensitivity of 0.160 kPa^{-1}.

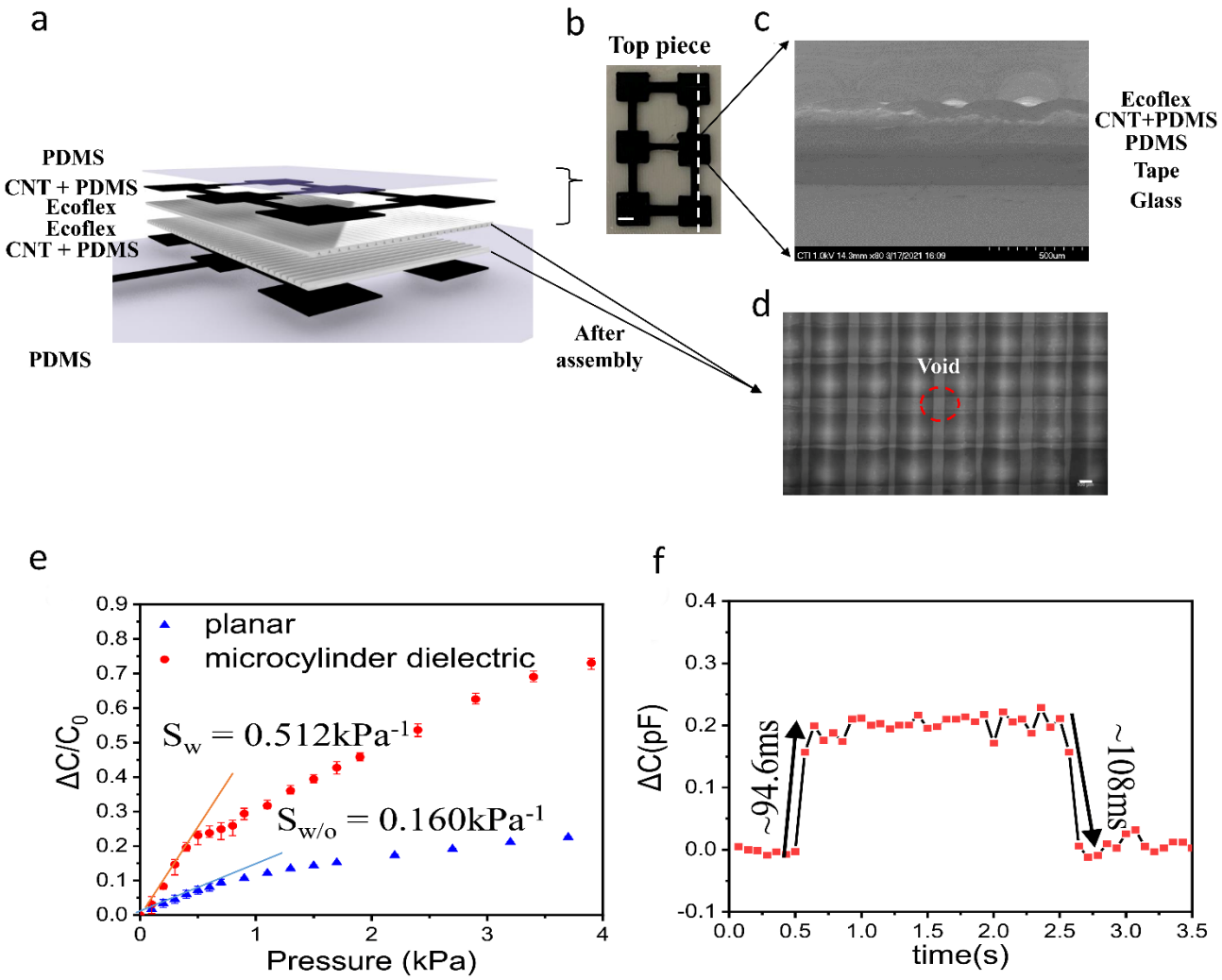

Figure 2.3: Structure of direct 3D printed microcylinder structure and sensor characteristic. (a) Layer schematics of the M2A3DNC sensors. (b) The optical image of the printed hemicylinder dielectric on the top of PDMS/CNT + PDMS substrate, scale bar: 2 mm. (c) The SEM image showing the cross-section of a 3D printed multilayers structure of Ecoflex 00-30, CNT + PDMS, and PDMS on a double-sided tape attached to a glass substrate, prepared for the cross-section imaging. (d) Microscopic image of hemicylinder dielectric grids, scale bar 100 µm. (e) Relationship of the capacitance change with the applied pressure from 0 to 4 kPa for the M2A3DNC sensors with and without microstructure patterned dielectric layer (five measured data points were collected for each pressure load). (f) The change in capacitance of the sensors upon applying a 5.4% bending strain followed by the strain release of one representative device.

2.3 Materials and methods

Preparation of CNT + PDMS Ink (12 wt%): 360 mg MWCNT (10–20 nm, 10–30 μm, Nanostructured and Amorphous Materials Inc, TX) is mixed with 7200 mg toluene (Certified American Chemical Society grade, Fisher Scientific, NH) at a weight ratio of 1:20. This blend undergoes magnetic stirring at a rate of 700 rpm for a duration of 2 hours. Concurrently, 2640 mg of PDMS (Sylgard 184 Silicone Elastomer Base, Dow Corning, MI) is integrated with 9486 mg of toluene (in a volume ratio of 1:4) for a similar time period. The prepared PDMS mixture is subsequently transferred to the CNT blend, subjected to baking at 50 °C, and stirred at 250 rpm to facilitate solvent evaporation. As the evaporation process nears completion, 264 mg of curing agent is incorporated into the mix. The entire blend undergoes further mixing using a Vortex mixer for an additional 20 minutes, and post this process, it is deemed ready for 3D printing.

Preparation of PDMS and Ecoflex ink: The base materials of SE 1700 (Dow Corning, MI) and Sylgard 184 are mixed with their respective curing agents in a 10:1 ratio, and this process is carried out for a duration of 10 minutes. Following the mixing, both blends are subjected to a degassing process in a vacuum desiccator for a period of 20 minutes. Subsequently, SE 1700 and Sylgard 184 are combined in a 2:1 ratio for 10 minutes, and this is followed by a centrifugation process at 4900 rpm for 20 minutes, facilitating the elimination of any potential bubbles. Part A is combined with Part B of Ecoflex 00-30 (Smooth-On Inc) in a 1:1 ratio, after which the blend undergoes a vortex mixing process for a period of 5 minutes. Subsequently, a centrifugation process at a speed of 2000 rpm is applied for a duration of 3 minutes. It's recommended that the ink is utilized within 40

minutes post-mixing to prevent alterations in viscosity brought about by curing.

Fabrication of Multi-material 3D Printed Sensor: The preparation of a sacrificial poly(vinyl alcohol) (PVA) layer starts by spin coating it onto a glass slide, which measures 7.5 cm in length, 5 cm in width, and 1 mm in thickness. The PVA solution, composed of a 1–10 weight ratio of PVA to DI water, is spin coated onto the glass slide at 1000 rpm for a duration of 60 seconds to yield a PVA layer with a thickness of 750 nm. This PVA layer undergoes a drying process on a hotplate, which is heated at 95 °C for 5 minutes. The subsequent 3D printing process for PDMS and CNT + PDMS starts with the creation of 3D patterns using Solidworks (Solidworks Corp). The slicing and generation of g-code is performed by Heartware (Cellink, MA), after which the defined patterns are printed via the Incredible+ 3D extrusion bioprinter (Cellink, MA). A conical nozzle with an internal diameter of 200 μm is utilized for PDMS ink extrusion, which occurs at a speed of 10 mm/s under a pressure of 80 kPa. The extrusion of CNT ink utilizes a stainless-steel nozzle with an inner diameter of 260 μm and happens at a speed of 7 mm/s under a pressure of 120 kPa. For Ecoflex 00-30 (Smooth-On, PA), a nozzle with an internal diameter of 100 μm is used and the extrusion occurs at a speed of 10 mm/s under a pressure of 4 kPa. The respective curing conditions for PDMS, CNT + PDMS, and Ecoflex 00-30 are as follows: 100 °C for 60 minutes, 100 °C for 60 minutes, and 80 °C for 30 minutes. Assembly of the sensor is achieved through the adhesive-like property of partially cured Ecoflex 00-30. The final step includes freeing the resulting sample from the substrate in a 90 °C water bath for 2 hours and then allowing it to dry in the air before it is ready for use.

Printing Parameters Optimization: The impact of printing resolution is evaluated by conducting tests at four pressures (90, 100, 110, and 120 kPa), seven speeds (ranging from

1mm/s to 7mm/s), and with three different nozzle sizes (0.51, 0.34, and 0.26 mm). Under each condition, five lines are printed repeatedly, with the average and the standard deviation of the printing result recorded. Measurements of the width and thickness are carried out using a Vernier Caliper.

Sensor Performance: The pressure control is performed by TA Q-800 Dynamic Mechanical Analyzer, and the data are collected by LCR meter and plotted by Origin software.

Chapter 3

A 3D-printed, Wireless, Battery-free, and Wearable pH Sensor System for On-demand Personal Health Monitoring

3.1 Introduction

Wearable biosensors currently garner significant attention due to their potential role in the early diagnosis and assessment of disease states. This emerging technology could potentially revolutionize healthcare, particularly through the real-time monitoring of relevant biomarkers, hence enabling timely interventions with appropriate therapeutics. Innovative devices aim to detect various biomarkers that are rich in physiological information, including lactate, glucose, pH, and the human chorionic gonadotropin hormone.[24]–[27]These biomarkers are obtained from various body fluids, such as sweat, urine, tears, saliva, and interstitial fluids.[28]

Among these biomarkers, pH serves as a straightforward yet crucial indicator of health conditions, given that it carries important health information from biofluids. For instance, changes in wound pH, from a less acidic state (pH 5.5 – 6.5, which is typical of normal healthy skin) to a more alkaline one (pH 7.15 – 8.9), can indicate various health-related processes.[29], [30] These include the release of different enzymes, acids, and ions linked with cell apoptosis and tissue remodeling. Notably, communities with low to medium resources bear a disproportionate burden of chronic wounds and lymphoedemas. Thus,

there is a significant need for accurate and cost-effective systems to monitor pH levels in real-time.

Furthermore, the pH in body fluids can shed light on vital enzymatic reactions associated with tumor metastasis, as well as critical processes involved in cell growth.[31] Specifically, cell growth is regulated by the proton (H+) content, produced by organic acids present in living cells.[32] Therefore, real-time monitoring of the pH in biological fluids could potentially provide critical early-stage information for the detection of disease onset, progression, and resolution, thereby enabling life-saving therapeutic interventions.

Near Field Communication (NFC) technology facilitates wireless and battery-free operations, enabling continuous and on-demand in-situ monitoring. It allows for the wireless transmission of both power and data when linked with a smartphone. NFC technology could potentially obviate the need for onboard lithium-ion or alkaline batteries, thereby facilitating system miniaturization and mitigating potential toxicity.[33] With NFC technology, measurements can be recorded and displayed on custom-designed applications via the NFC module on a smartphone. By harnessing the ubiquity of modern smartphones, NFC technology presents a significant opportunity to advance personalized healthcare. It provides wearable and portable systems for on-demand, continuous data acquisition. Moreover, NFC technology could prove instrumental in effectively monitoring personal healthcare, whether at home or in low-resource settings. The technology offers the potential for portable devices that are compact, cost-effective, and user-friendly, demonstrating the breadth of its utility and its capacity to reshape healthcare monitoring and delivery.

The emergence of additive manufacturing, commonly known as 3D printing, introduces a more readily available and economically viable option compared to traditional manufacturing methods. Additive manufacturing is a technique that builds objects by

successively depositing material in layers, in accordance with a pre-determined digital model. Unlike conventional fabrication methods, which rely on the removal of material to construct a shape, additive manufacturing utilizes only the required material to form the object, which not only reduces waste but also enables the creation of more intricate designs. These innovative techniques are more user-friendly, expedited, and economically beneficial compared to traditional clean-room-based microfabrication methods.[34]–[36]

A notable advantage of 3D printing is its capacity to print multi-material, multi-layer structures, which is a revolutionary feature to produce wearable sensors. It facilitates the simultaneous integration of diverse materials with a variety of properties into a singular device. Furthermore, 3D printing grants the flexibility to modify the viscosity of the utilized materials and to choose from an extensive array of materials based on the desired application. These capabilities pave the way for fresh opportunities in the design and manufacturing of wearable sensors, allowing for the development of more sophisticated, functional, and efficient devices.[6], [12]

In this context, over the last few years, the development of wearable pH sensors for in-situ, real-time monitoring of body fluid pH has been advanced. The aim is to improve health condition monitoring. However, conventional sensors face several challenges when it comes to personalizing wearable pH sensors for human healthcare monitoring. A wearable pH sensor must meet certain criteria, including sensor flexibility and stability, time and cost-efficiency in fabrication, low power consumption and continuous measurement, biocompatibility or wearability, and the provision of valuable and timely information to the wearer.

In order to address these concerns, we present a wireless, battery-free, biocompatible, flexible, 3D-printed (W2BF3D) wearable pH sensing system that integrates

with a near-field communication (NFC) readout. Our system consists of two components: a disposable pH sensor and a reusable NFC readout system, allowing for real-time pH monitoring directly from sweat. The W2BF3D pH sensor and NFC circuit are fabricated on a styrene-ethylene-butylene-styrene (SEBS) substrate and polyimide film, respectively, providing flexibility. Specifically, the SEBS material possesses mechanical properties similar to human skin, including a Young's modulus of approximately 0.2 MPa, offering excellent flexibility and stretchability of up to 300%.[37] To fabricate the pH sensor, NFC electronic circuit, and NFC antenna, we employed a direct ink writing technique using a 3D printer. This 3D printing method is widely recognized for its efficiency, cost-effectiveness, and simplicity compared to traditional 2D planner processes used in wearable sensor development. Additionally, the integration of the NFC readout system with the W2BF3D pH sensor enables wireless and battery-free operation, allowing for continuous in situ monitoring. The measurements are transmitted to a connected smartphone through the NFC module, where they can be recorded and displayed on a custom-designed app. Leveraging the prevalence of smartphones presents significant opportunities to advance personalized healthcare by providing wearable and portable systems for continuous data acquisition. Moreover, these portable devices with small size, low cost, and ease of use have the potential to greatly improve personal healthcare monitoring in various settings, including home and low-resource environments. The W2BF3D wearable pH sensor exhibits remarkable sensitivity, specificity, repeatability, and reproducibility across various pH ranges (5.5 – 7.0), while maintaining mechanical stability and flexibility. The sensor also successfully passed a bending test of up to 500 cycles. Compared to the previously reported drop-casted PANI-based sensor, our pH sensor demonstrates high sensitivity (~ -29.45 mV/pH) with a correlation coefficient of 0.999. To assess the potential of skin inflammation resulting from

long-term interaction with human skin in on-body applications, we conducted a biocompatibility test of the W2BF3D wearable pH sensor. The test involved culturing murine myoblast (C2C12) cells on the sensor for 5 days, resulting in 90% cell survivability. Additionally, we validated its usage in an ex-situ hydrogel-based wound model, monitoring real-time wound healing by measuring pH changes (from 7.0 to 4.0). The on-body test demonstrated the successful ex-situ and in-situ measurement of pH values in artificial and actual sweat in a wireless manner. Overall, our W2BF3D wearable pH sensing system offers a comprehensive platform for accurate and wireless measurement, enabling real-time human healthcare monitoring that is simple, efficient, cost-effective, and non-invasive, while minimizing discomfort.

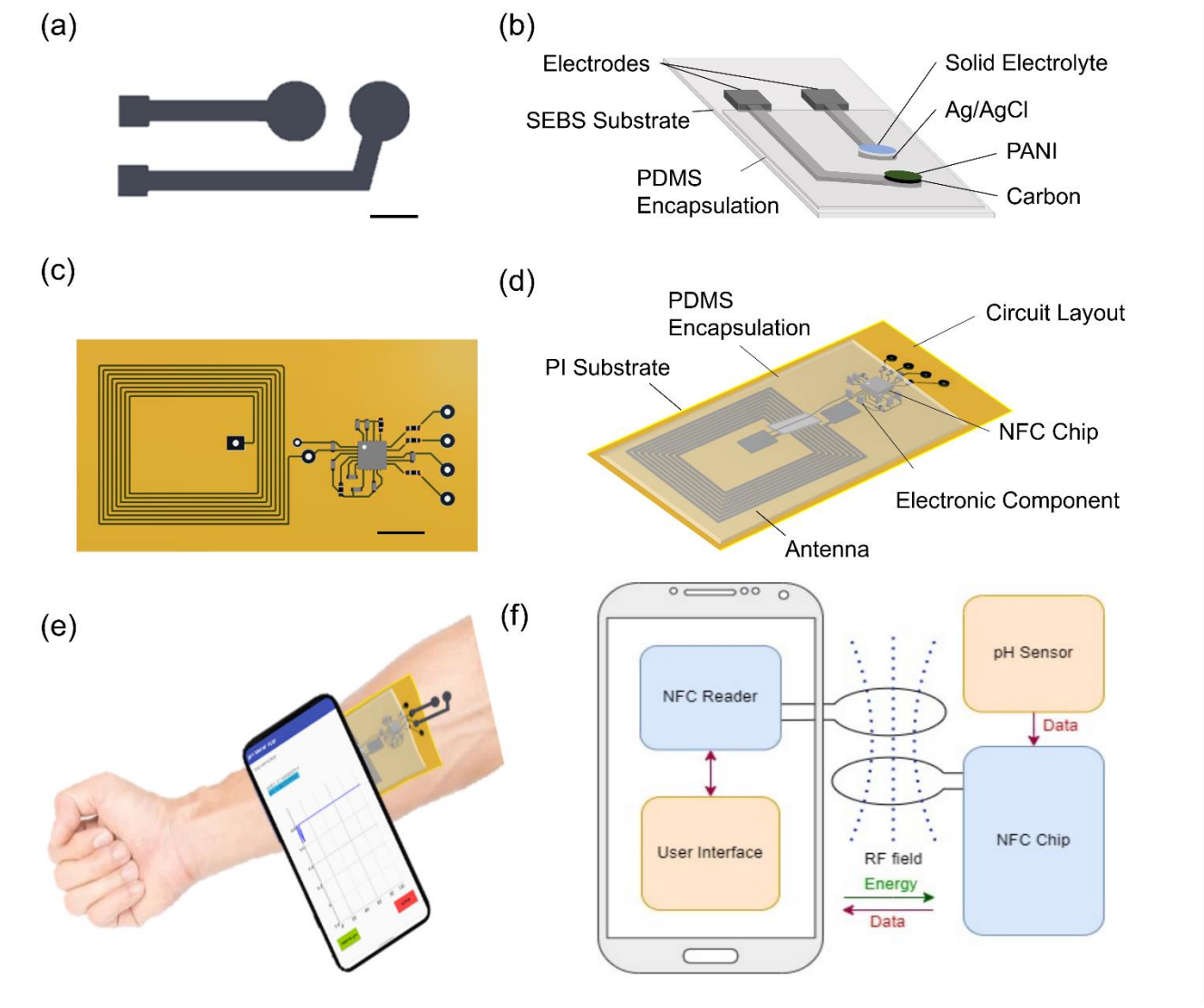

Figure 3.1: Schematic diagrams of the WB2F3D sensor system. (a) Top view design of electrode of the pH sensor (scale bar: 3 mm). (b) A schematic image of the pH sensor that shows the multiple modification layers of the working electrode and reference electrode. (c) Top view design of NFC electronic circuit (scale bar: 1 cm). (d) A schematic of the NFC electronic circuit which is encapsulated using PDMS. (e) The illustration shows the concept of an on-body test with the WB2F3D sensor system. (f) A block diagram shows the Near Field Communication between the readout system of the pH sensor and a smartphone, enabling to perform the pH sensing without any external power source. The results will be displayed on the smartphone App.

3.2 Results and Discussion

3.2.1 Design and fabrication of the WB2F3D sensor system

Figure 3.1a–f presents each component (module) of the proposed wireless, wearable, battery-free, biocompatible, flexible, and 3D-printed (WB2F3D) sensor system in current use. Figures 3.1a and b depict the design schematics of the pH sensors module from an overhead view. The sensor incorporates a circular-shaped working electrode (WE) and a reference electrode (RE), both of which are based on silver. The WE receives a coating of carbon and Polyaniline (PANI) films, while the RE gets layered with Ag/AgCl and solid electrolyte. The conductive layers are ensconced within PDMS, leaving the sensing areas exposed. The sensor's operation is based on the well-established principle of protonation of a nitrogen atom in PANI polymer chains.[38] Notably, the PANI exhibits high electrical conductivity in acidic solutions when the polymer is doped with H+ ions, thereby generating the emeraldine salt form of PANI.[39] Consequently, the disparity in surface charge between the WE and the RE results in an observable electrical potential difference, associated with the pH level (H+ concentration) of the surrounding solution. As expected, the surface charge diminishes as the H+ ions neutralize in alkaline solutions.

Figure 3.1c delineates the preparation steps of the NFC-based electronic/communication circuitry module. The NFC-based electronic/communication circuitry is designed as a multilayer structure with the electronic circuit sandwiched between PDMS and polyimide (PI) substrates. The NFC-based electronic/communication circuitry comprises a flexible inductive coupling spiral antenna, silver nanoparticle (AgNP) printed interconnections, insulation layers, and passive and active discrete components (i.e., NFC transponder IC, external capacitors), all encapsulated within PDMS (Figure 3.1d). Figure 3.1f presents the block diagram of the NFC-based electronic/communication circuitry. As illustrated, power and data transmission take place from the proximity of the reader antenna (i.e., smartphone) to the circuitry module antenna via inductive coupling. The energy

harvested by the NFC chip's power management unit is regulated into a stable voltage output (≈1.5 V), which powers the circuitry module of the WB2F3D sensor system. Following this, the system reads the sensor's open circuit potential in real-time (using the onboard NFC chip's 14-bit sigma-delta analog-to-digital converter (ADC)) and wirelessly transmits it to a smartphone. The communicated data are then displayed on a custom-developed user interface (Android App) (Figure 3.1e).

The fabrication procedures of the PANI-based pH sensor are illustrated in Figure 3.2a. In summary, the SEBS/PVA substrate is prepared by spin-coating polyvinyl alcohol (PVA) on a glass slide, followed by casting of SEBS. The fabrication process continues with the 3D printing of a silver nanoparticle-based ink on a flexible PI substrate and its curing at 80 °C for 20 minutes to fabricate the NFC-based electronic/communication circuitry module (including the antenna and the footprint of the NFC transponder chip) in a layer-by-layer approach (Figure 3.2b, c). A custom Android App acts as the user interface to receive, process, display, and store measurement data on a smartphone when it is in close proximity (≈2 cm) to the WB2F3D sensor system.

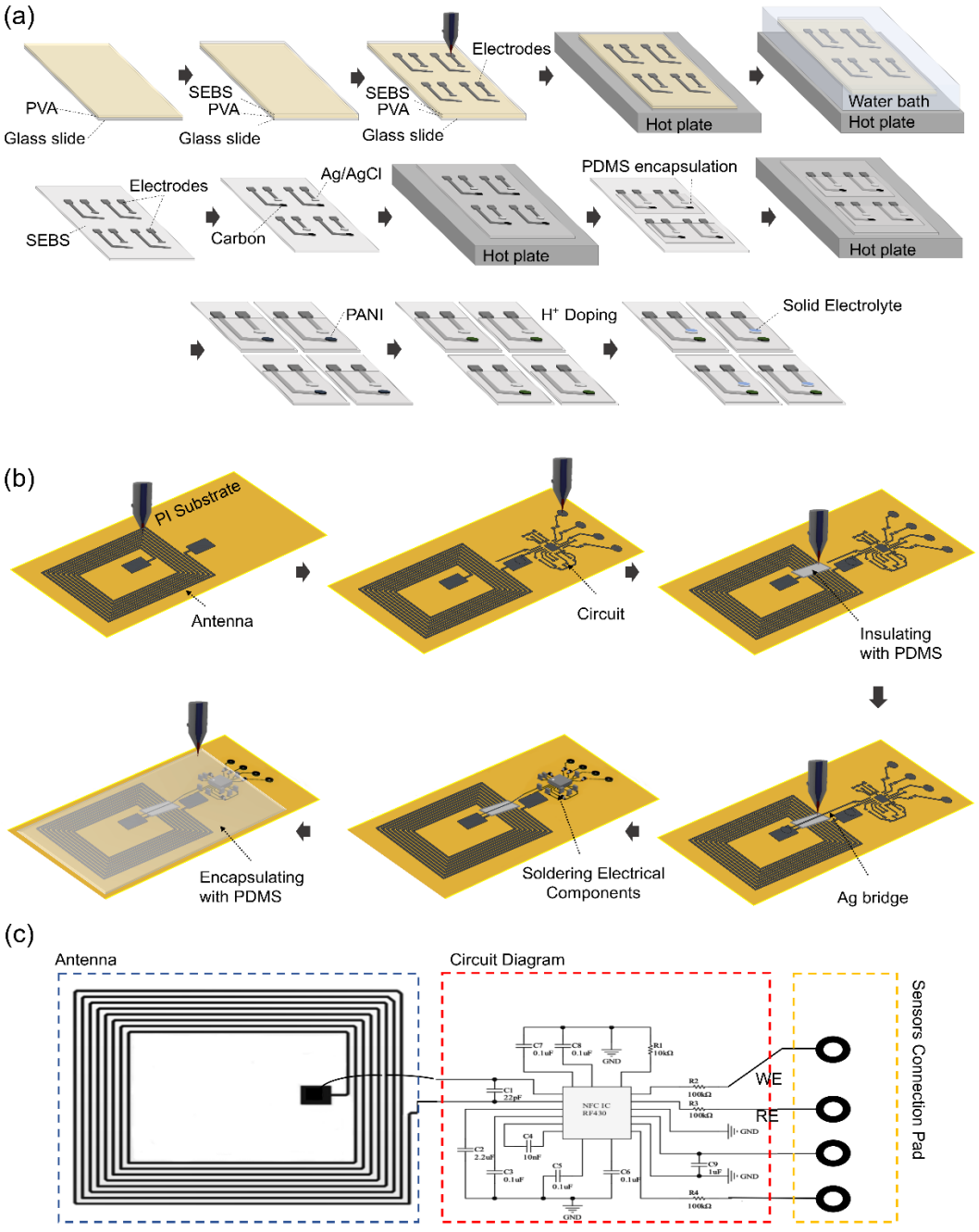

Figure 3.2: Fabrication procedures of the WB2F3D sensor system. (a) The pH sensor module of the WB2F3D sensor system fabrication steps on skin-like SEBS substrate. (b) The reusable and flexible NFC-based electronic/communication circuitry module of the WB2F3D sensor system including the antenna and the footprint of the NFC transponder chip; 3D-printed on the flexible PI substrate for the on-demand, wireless, and battery-free operation in a wearable format. (c) The circuit diagram of the NFC-based electronic/communication circuitry of the WB2F3D sensor system connected to the sensors and antenna.

3.2.2 Morphological Characterizations

Using a field-emission scanning electron microscope (FE-SEM), the working electrode (WE) and reference electrode (RE) of the sensor system are examined for morphological characterization, as depicted in Figure 3.3. The SEM image displays the WE surface uniformly coated by the PANI layer (Figure 3.3a), indicating the precision of the coating process.[40] However, the RE image (Figure 3.3b) does not present any distinguishable features. Observing the cross-sectional image, we can affirm that the PANI, with a thickness of about 120 μm, is well deposited on the carbon substrate (Figure 3.3c). In parallel, the SEM image of the RE confirms the application of a solid electrolyte layer of optimal thickness (averaging 150 μm) onto the Ag/AgCl (Figure 3.3b, d).

The solid electrolyte's placement on the RE supplants the inner electrolyte and liquid junction found in typical Ag/AgCl reference electrodes, facilitating rapid stabilization of the sensors before they are employed for sensing. Existing literature suggests that the thickness of the solid electrolyte layer plays a significant role in determining the RE's lifespan, being governed by the rate of NaCl leakage through diffusion at the intersection of the electrode's polymer matrix and the test solution.[41] Hence, a more substantial solid electrolyte suggests a longer projected RE lifespan.[41] However, the downside of an increased solid electrolyte thickness is a more extended time required for the sensor to stabilize and a reduction in mechanical flexibility. These findings underscore the criticality of optimizing the thickness of the RE (the total of the solid-electrolyte thickness and the silver nanoparticle electrode thickness) to ensure a wearable pH sensor that is not only stable and fast-reacting but also mechanically flexible.

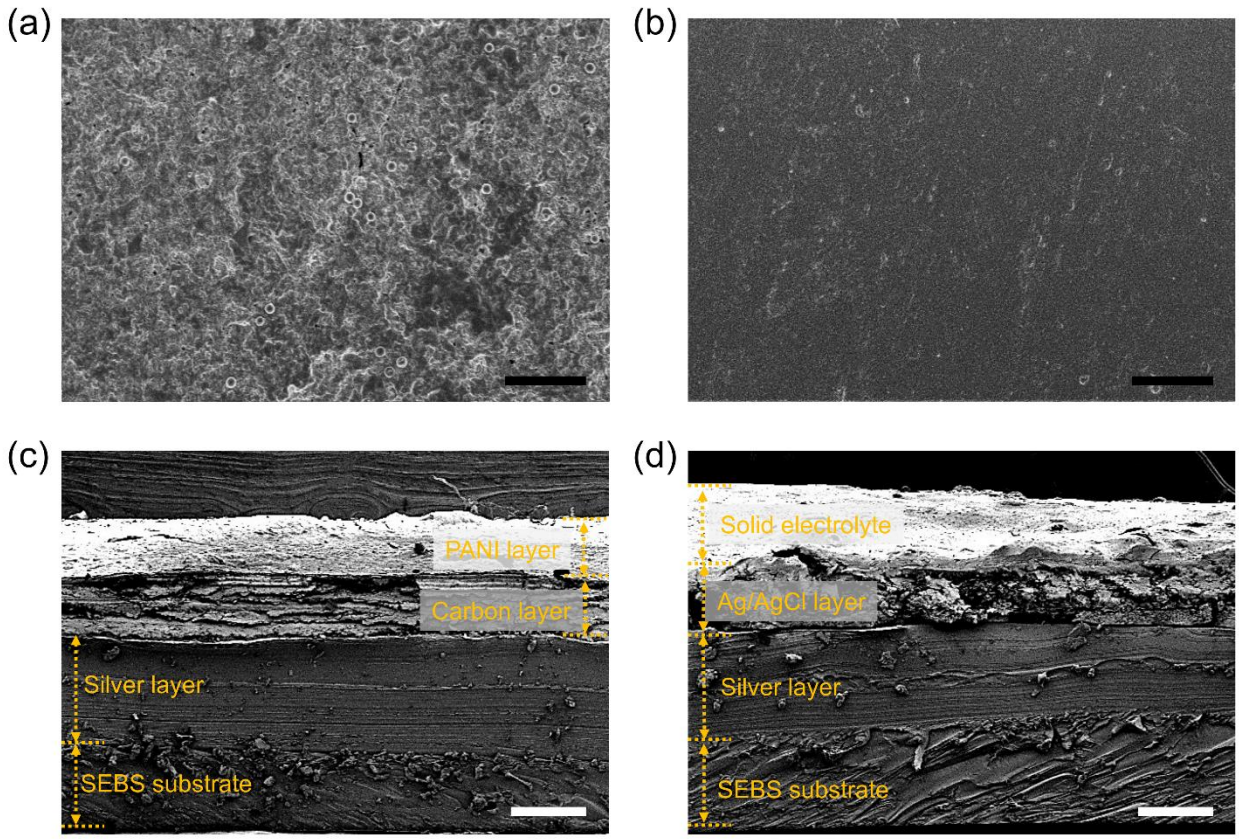

Figure 3.3: FE-SEM images of working and reference electrodes. Bird eye's view image of a) the working electrode and b) the reference electrode (scale bar: 3 µm). Cross-sectional image of c) the working electrode and d) the reference electrode (scale bar: 200 µm).

3.2.3 Ex Situ Characterization of the WB2F3D Sensor System

The individual components of the WB2F3D sensor system (the single-use pH sensor module and the reusable NFC-based electronic/communication and antenna module) are currently being characterized and validated to assess system performance. The pH sensor module's performance (open circuit potential versus pH values) is being meticulously analyzed, as illustrated in Figure 3.4. The pH sensor's sensitivity depends on the PANI polymerization on the WE.

While the frequently used electro-polymerization of PANI documented in the

literature displays sensitivity close to the Nernstian slope,[40] it carries several drawbacks. These include the use of a toxic aniline monomer and concentrated hydrochloric acid, plus the complexity of the process, making it a less than ideal choice for wearable applications. Alternatively, the method utilized in this study involves dissolving polyaniline emeraldine base in dimethyl sulfoxide (DMSO) and applying it to the working electrode, which results in enhanced biocompatibility, sensitivity, and affordability.[42]

The WB2F3D sensor system is demonstrating high repeatability and sensitivity across different pH ranges, as depicted in Figure 3.4a, b. Predictably, as the pH level rises, the measured potential decreases, correlating with the PANI's protonation and the concentration of H+ ions. Conversely, the potential rises as the pH level falls. Figure 3.4b reveals the sensor's linear response, with a Nernstian sensitivity (approximately -51.76 ± 0.97 mV/pH) and a correlation coefficient (R^2) of 0.997. The sensitivity of this 3D-printed sensor aligns with previously reported drop-casted PANI-based pH sensors and exceeds that of screen-printed PANI-based pH sensors.

The pH sensor's selectivity is being tested with various potential interfering electrolytes and metabolites, such as CaCl2, KCl, NaCl, and glucose, as portrayed in Figure 3.4c. These interferences are prepared to their physiologically relevant concentrations and adjusted to pH 7. As Figure 3.4c shows, the sensor only reacts to changes in pH, demonstrating high specificity.

Mechanical flexibility, a crucial factor in reducing discomfort and mechanical stress caused by body movements in wearable devices, is also being evaluated. A cyclic bending test of up to 500 cycles is being conducted, with the sensor's performance at different pH ranges (from 3.0 to 10.0) being assessed before and after bending. For these tests, the sensor is

attached to a linear motor, with repeating bending and release cycles applied (Figure 3.4d, inset). The average bending of sensors when fixed to a human wrist is approximately 1% with a bending radius of 30 mm.[43] However, the bending test in this study is carried out under a harsher condition of 16% bending, for 500 repeated bending and releasing cycles. As depicted in Figure 3.4d, the sensor maintains a reliable performance with no significant change (<2.5% variations), showing it has high flexibility to be worn comfortably and reliably on the human body.

Next, the wireless power transmission reliability of the NFC-based electronic/communication circuitry module is being evaluated under different bending tests. The NFC chip's voltage output remains stable at roughly 2.17 V while the circuit undergoes various bending radii ranging from 5 to 30 mm, as shown in Figure 3.4e, indicating negligible or very slight (<1%) power loss and reliable power transmission of the NFC-based electronic/communication circuitry module. To further assess this module's reusability, reliability, and stability, various potentials are applied to the ADC pins of the NFC-based electronic/communication circuitry module and recorded before and after repeated bending and release cycles (ten bending cycles at 30%). As demonstrated in Figure 3.4f, the transferred voltage difference before and after the 30% bending is negligible (<1%), confirming the NFC module's stability and reusability for repeated usage on the human body.

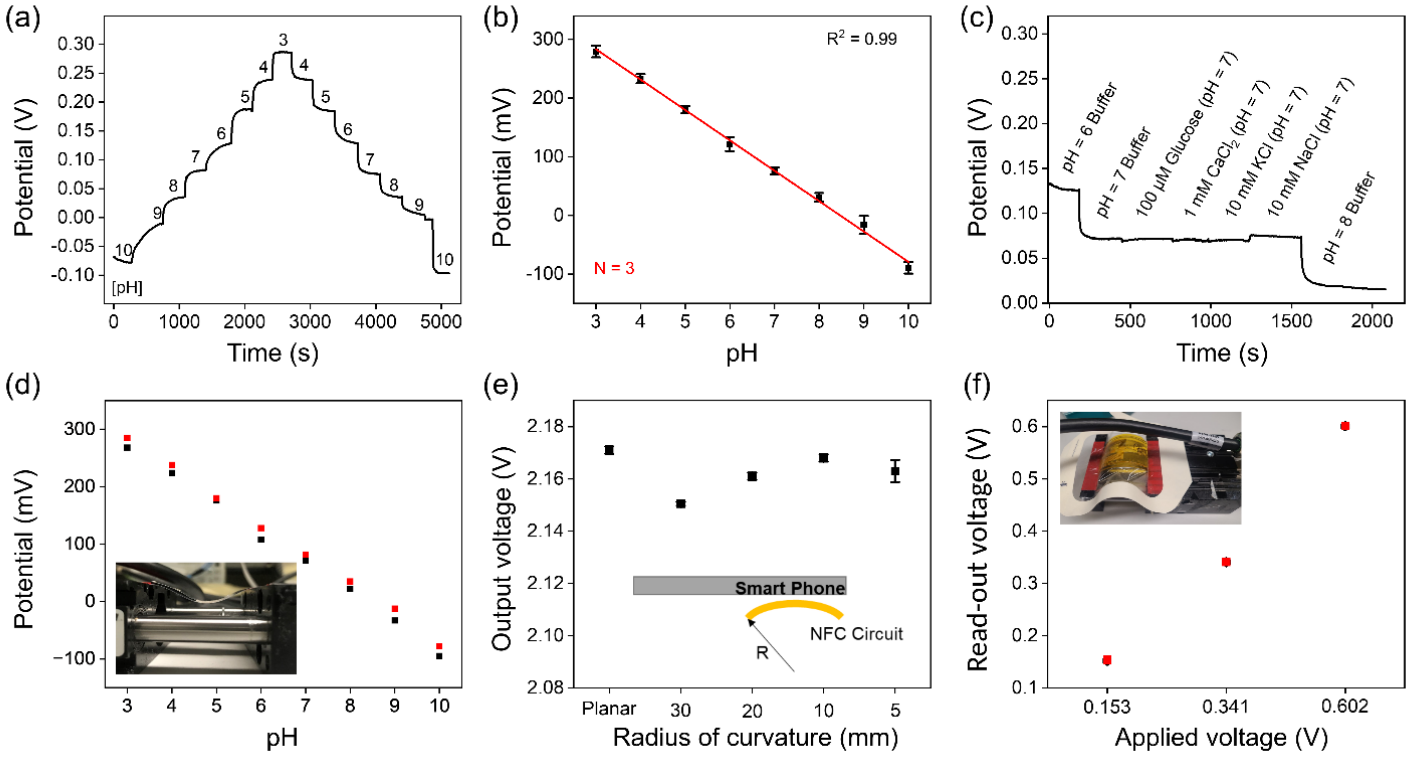

Figure 3.4: Electrical performance characterization of the WB2F3D sensor system. (a) Open circuit potential versus pH ranging from 3.0 to 10.0. (b) Linear calibration curve of the sensor and (c) the selectivity evaluation of the sensor. (d–f) Mechanical characterizations of the sensor under the ex-situ bending tests. (d) The sensor's performance evaluation before (black dot) and after (red dot) applies 500 cycles of bending (at 16% bending) and releasing. The inset image shows a side view of the experimental setup for the cyclic bending test using a linear motor. The sensor showed a reliable performance with no significant change (<2.5%). (e) The rectified voltage output of the NFC chip with different bending curvatures of the NFC antenna. (f) NFC exchanged voltage to the phone before (red dot) and after (black pentagon) ten cycles of bending and releasing compared to the applied voltage demonstrating no significant change (<1%). Each data point represents triplicate measurements.

3.2.4 In Situ Wireless and Real-Time pH Monitoring

The WB2F3D sensor system is undergoing validation for on-site, real-time, wireless, battery-free, and on-demand pH monitoring, as depicted in Figure 3.5. In the initial set of experiments, prior to testing the device against actual sweat, synthetic sweat samples are prepared. These samples are mixed with various interfering ions, and their pH levels are

adjusted to a range of physiologically relevant pH values (4.0–8.0). Following this, the WB2F3D sensor system is attached to the human forearm skin (see Figure 3.5b), the samples are applied to the skin, and the on-site measured pH values are wirelessly transmitted to the smartphone via the integrated NFC circuitry module, which are then displayed on a custom-built Android app (as shown in Figure 3.5c, d). These experiments help establish the calibration curve of the WB2F3D sensor system against various pH levels, which exhibits good linearity (R^2 = 0.99), as seen in Figure 3.5a. This curve is subsequently used to discover the reverse transfer function of the WB2F3D sensor system, enabling the calibration and re-programming of the app for on-site and wireless pH measurements of actual human sweat samples.

The next step involves on-site pH monitoring of real human sweat to test the practical applications of the WB2F3D sensor system. For this, a volunteer is asked to wear the WB2F3D sensor system and exercise for approximately 30 minutes to generate sweat. The phone is then brought near the NFC module of the WB2F3D sensor system to wirelessly exchange power and activate the system, thus enabling wireless, on-demand, and real-time pH monitoring (shown in Figure 3.5f). A control experiment is conducted simultaneously, where the same sweat sample is collected. As Figure 3.5e shows, the pH value reported by the WB2F3D sensor system for the actual sweat from the on-site measurements is pH = 6.80, and the pH value measured by the commercial pH sensor from the simultaneously collected sweat sample is pH = 6.58 (see Figure 3.5f). The difference is approximately 3.3%, demonstrating the accuracy and reliability of the proposed WB2F3D sensor system for on-demand, wireless, battery-free, and real-time on-site pH monitoring in a wearable format.

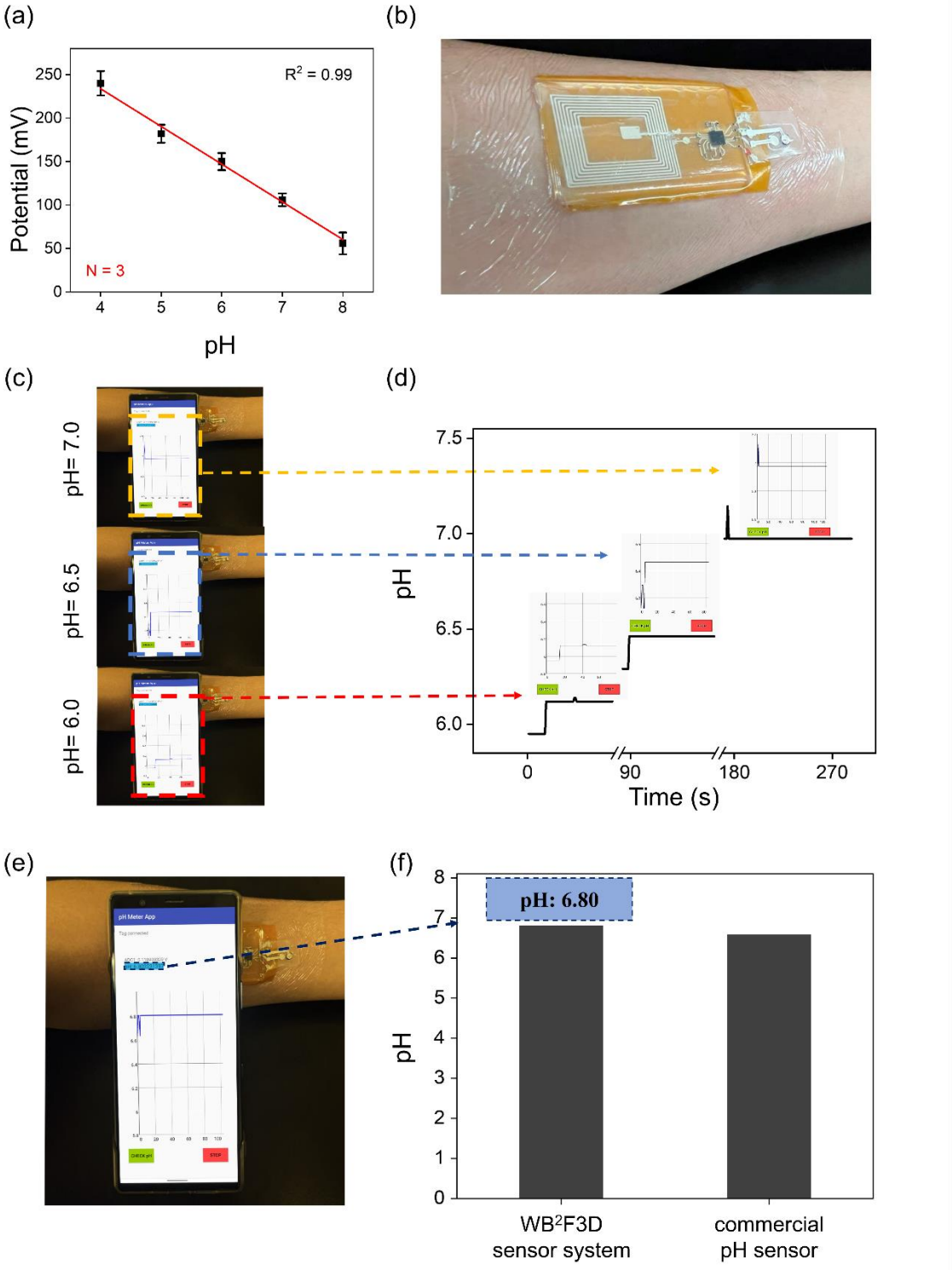

Figure 3.5: Real-time, in situ, battery-free, and wireless pH monitoring using the WB2F3D sensor system. (a) The calibration curve of the WB2F3D sensor system against various ranges of pH (4.0–8.0) in an artificial sweat sample. b) Photo of the WB2F3D sensor

system attached to the human forearm for the real-time and wireless pH measurement of pH changes. c) Real-time, battery-free, on-demand, and wireless measurement of various pH levels ranging from 6.0 to 7.0 in an artificial sweat sample. d) A phone displaying measured pH values of the applied artificial sweat applied to the skin. The insets were extracted from (c). e) In situ and real-time measurement of the forearm's actual sweat pH value. f) The bar graph comparing the forearm's sweat pH value measured and reported by the WB2F3D sensor system and by a commercial pH sensor (from a same time collected sweat sample). The difference is negligible 4 exhibiting the capability of the WB2F3D sensor system for accurate and reliable in-site pH measurements and wireless data and power transmission.

3.2.5 Biocompatibility Validations and Simulated Wound Model

We have conducted a comprehensive biocompatibility evaluation of the system to ascertain its potential usage in monitoring wound healing (see Figure 3.6). The first step involves testing biocompatibility by cultivating NHDFs (obtained from human skin) on the sensors and tracking their viability and metabolic activity for a period of 7 days. The live/dead assays (on days 1, 3, and 7) demonstrate a cell viability of at least 90% in the samples, illustrating the impressive biocompatibility of the sensors (shown in Figure 3.6a). More specifically, the viability rates are quantified as 91.8 ± 6.5%, 91.3 ± 1.3%, and 90.8 ± 2.2% on days 1, 3, and 7, respectively (as shown in Figure 3.6b). In addition, we monitor the metabolic activity of the cultured cells for 7 days, which shows a gradual increase (Figure 3.6c), indicating expected cell proliferation in a highly biocompatible environment. These results validate that the sensors meet the cytocompatibility requirements, exhibiting excellent biocompatibility, making them ideal for wearable applications and in situ pH monitoring.

Furthermore, we have developed an ex situ hydrogel-based wound model to simulate the wound healing/infection processes. During these processes, the pH of the wound typically transitions from 4.0 to 7.0.[44] In our model, we mimic the dynamic pH changes during these processes based on the time it takes for ions to diffuse into the hydrogel-based wound model and alter its initial pH level (set at pH = 7) to a new pH level (pH = 4). We have also optimized

the thickness of the hydrogel to about 5 μm, enabling us to record pH level changes in the model in real time. In these experiments, we first place the wound model with a pH 7 on the sensor (Figure 3.6d, e), followed by the application of a serum sample at pH 4 to the opposite side of the wound model. The ions then gradually diffuse into the hydrogel, resulting in a change in pH over time (Figure 3.6e) in the model and at the sensor-hydrogel interface. It takes approximately 34 minutes for the pH level at the sensor-hydrogel interface to completely change and reach the new pH level of pH = 4 (Figure 3.6e). This experiment is designed to represent a fast-forwarded version of the wound healing/infection process, which is successfully monitored by our sensors. These results suggest that our sensors have considerable potential for real-time wound healing by tracking dynamic pH level changes over time. However, wound healing can span several days to weeks, and any sensor used for this purpose should be capable of long-term contact with the wound sites without frequent replacement. Therefore, further studies will be required to assess the extended usage and on-site wound healing monitoring capabilities of our sensors, which will be the direction of our future research on this topic.

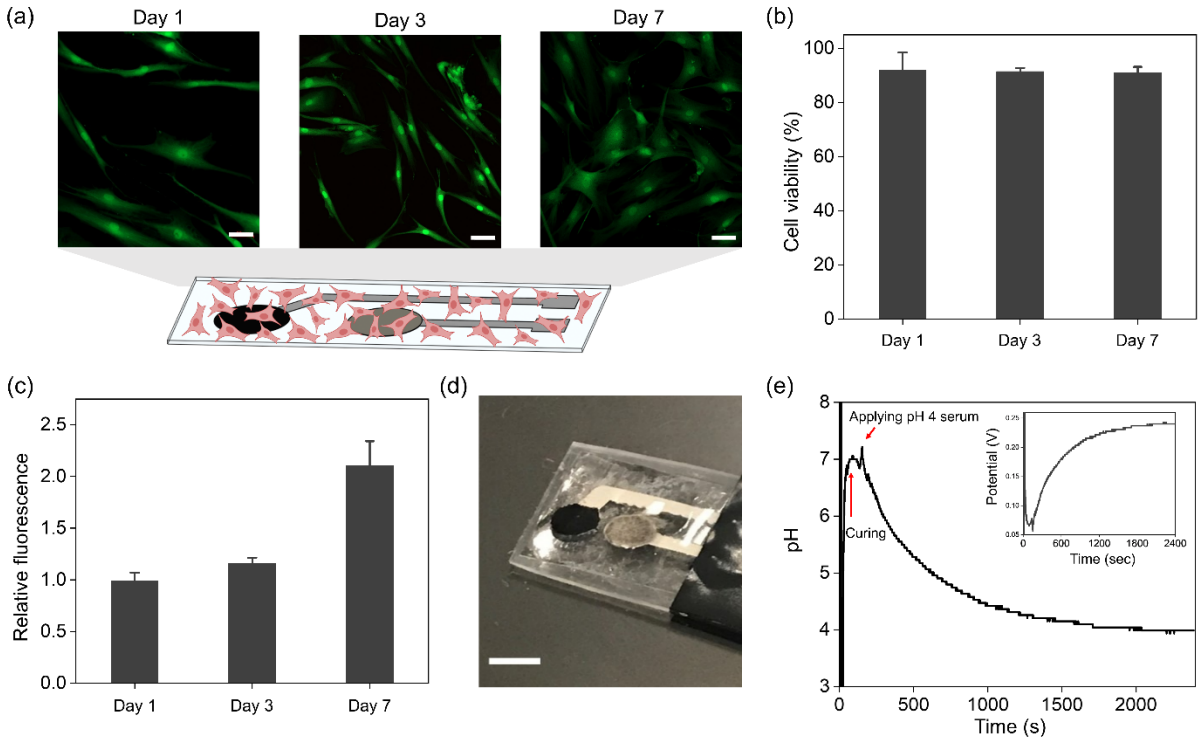

Figure 3.6: Biocompatibility assessment of the WB2F3D sensor system. (a) Image representatives of live/dead fluorescent micrographs of normal human dermal fibroblast cells cultured for 7 days on the pH sensor showing the cell viability on 1, 3, and 7 days of the culture (scale bar: 50 µm). b) Viability quantification of fibroblast cells assessed by calcein-AM/EthD-1 on days 1, 3, and 7 of culture with >= 90% viability rate. These cells were analyzed in three biological replicates. c) Metabolic activity assay on days 1, 3, and 7 of culture. These cells were analyzed in three biological replicates. d) The experimental setup for the dynamic pH monitoring in the GelMA hydrogel wound models (scale bar: 3 mm). e) Real-time pH monitoring in an ex situ hydrogel-based wound model when its pH changes from 7 to 4 over time, representing the dynamic pH changes, from 4 to 7, during the wound healing/infecting process. A serum sample at the pH = 4 was applied to the wound model (initially at pH = 7) which results in the wound model's pH change by time due to the ions diffusion. The inset shows the potential increase due to the dynamic pH change in the wound model from 7 to 4.

3.3 Materials and Methods

Preparation of pH Solutions and Artificial Sweat: We prepare a variety of solutions at different pH levels (ranging from pH 3.0 to 10.0) by combining HCl and KOH with distilled water. Before every experiment, we ensure the pH level of these solutions using a

commercial pH meter (Hanna Instruments Edge, USA). To simulate sweat for the wearable sensor experiments, we prepare artificial sweat based on the ISO 3160-0 method.[43] This involves mixing several components into distilled water, including 20 g/L of NaCl, 17.5 g/L of NH_4Cl, 5 g/L of acetic acid, and 15 g/L of lactic acid. We use a 150 g/L NaOH solution to adjust the pH values (for example, to 6.0, 6.5, and 7.0). The pH of the prepared artificial sweat is confirmed using the commercial pH meter.

PDMS Ink Preparation: The process for preparing PDMS ink is currently being carried out based on previous studies.[17] Briefly, we mix both SE 1700 (Dow Corning, MI) and Sylgard 184 base materials with their respective curing agents for 10 minutes at a 10:1 ratio, before degassing in a vacuum for 20 minutes. The degassed SE1700 and Sylgard 184 are then combined in a 2:1 ratio to finalize the ink composition, a process taking around 10 minutes. We then centrifuge the mixture at 4900 rpm for 20 minutes to eliminate any remaining bubbles.

Sensors' Fabrication: The working and reference electrodes, circuit interconnects, and antenna are 3D-printed using a flexible silver-nanoparticle-based ink (Flex 2 Conductive Ink, Volterra, Canada) on a flexible substrate with an extrusion 3D printer (Inkredible+, Cellink, USA). The printing process commences with the development of 3D patterns using Solidworks (Solidworks Corp., USA) and Altium Designer, followed by slicing and generating G-code through Heartware (Cellink, MA, USA), with additional G-code adjustments for printing accuracy. We prepare the PANI solution by dissolving 25 mg of polyaniline emeraldine base in 10 mL of DMSO, ensuring a uniform coating on the surface of carbon electrodes. Notably, the PANI emeraldine base is soluble in organic solvents such as DMSO, while PANI itself is insoluble in typical organic solvents.[45] We ultrasonicate the mixture of

PANI and DMSO for 2 hours and stir it continuously for 24 hours using a magnetic rod. Then, the solution is filtered using a 500 nm porous filter (Whatman filter) to obtain a uniform dark blue solution. We then drop-cast 4 μL of PANI solution on the carbon electrode and dry it slowly at 50 °C for 2 hours. Next, the polyaniline film is doped with H+ ions by placing the device in a vacuum chamber with 2 mL of 1 m HCl for 5 hours. The HCl fumes generated by the low pressure in the vacuum chamber introduce H+ ions into the polyaniline emeraldine-based membrane, converting it into polyaniline emeraldine salt. We rinse the electrodes with DI water and dry them with nitrogen. To prepare the RE, a PVB reference cocktail is mixed by combining 395.5 mg of PVB and 250 mg of NaCl in 5 mL of methanol. We then drop-cast 4 μL of this solution onto the RE. The modified electrode is left to dry overnight in the dark. However, to achieve optimal performance, the RE is conditioned with a 50 × 10−3 m NaCl solution for 3 hours before measurements. This conditioning process is vital for minimizing potential drift.

Sensors' Characterization: The surface of the pH sensors undergoes optical characterization using an FE-SEM (Hitachi 4700, Japan). To capture high-resolution images, a thin gold layer of about 10 nm is sputtered on the center of both electrodes, namely the WE and the RE. The electrical characteristics of the pH sensors are determined using a potentiostat (VersaSTAT 3, Princeton Applied Research). During the measurements, both electrodes are immersed in 100 μL of a pH solution. The potential is then calculated by measuring the open circuit potential between the WE and RE. Throughout the measurements, solutions of various pH ranges (pH 3.0–10.0) are continuously applied to the sensors. These experiments are carried out at room temperature, approximately 24 °C.

Fabrication and Characterization of NFC Electronic Circuit: The NFC-based

electronic/communication circuitry is comprised of an NFC transponder IC (RF430FRL152H, Texas Instruments), surface mount resistors, and capacitors. These components are soldered onto the silver nanoparticle 3D-printed footprints using a low-temperature solder paste (SMDLTLFPT5, Chip Quik). After the soldering step, the circuit undergoes re-heating on a hot plate at 135 °C for 2 minutes for reflow purposes. The electronic circuitry module is encapsulated by 3D-printing PDMS ink with nozzles of 0.6 mm inner diameter at a printing pressure of 100 kPa. The PDMS ink is then cured at 60 °C for 1 hour. The electromagnetic properties of the NFC antennas are characterized by a high-frequency impedance spectroscope (HF2IS, Zurich Instruments), which scans the frequency range from 100 kHz to 22 MHz.

Mechanical Characteristics of the WB2F3D Sensor System: The sensors attach to a linear motor system (Linmot motor, NTI AG), and they undergo cyclic bending and releasing tests at a 16% bending ratio for 500 cycles of 1 second bending and 1 second releasing. The time interval between two consecutive cycles is 3 seconds. The linear motor operates at a maximum speed of v= 0.05 m/s, acceleration of a=1 m/s^2, and deceleration of d = 1 m/s^2. The sensors' performance is examined both before and after bending, across various pH ranges from 3.0 to 10.0. The NFC-based electronic/communication circuitry module also undergoes an evaluation for wireless power transmission reliability under different bending tests. It mounts to a curved surface with varying radiuses of curvature, including 0, 10, 15, 20, and 30 mm. This is followed by applying different voltages to the ADC pin of the NFC-based electronic/communication circuitry module, which is read by the smartphone before and after repeated bending and releasing cycles. The bending cycle is set to 10 bending cycles at a 30% bending rate for 1 second and releasing for 1 second for ten cycles with 3-second

time intervals.

In Situ, Wireless, and Real-Time pH Monitoring: In the current process of in situ and real-time testing, the WB2F3D sensor system is attached to the subject's forearm using a stretchable and transparent 3M Tegaderm tape (F51CA07, 3M). The subject is instructed to exercise on a treadmill for 30 minutes to generate sweat. Simultaneously, in the control experiment, sweat is collected from the same subject, who is a healthy 27-year-old man. The pH value of the collected sweat sample is subsequently measured with a commercial pH sensor.

Biocompatibility Validations: NHDF cells in their early passages (less than 15) are being used. The pH sensors undergo sterilization with UV light for an hour before initiating any cell-related experiments. The NHDF cells are cultured in Dulbecco's modified Eagle medium (DMEM, Gibco), enriched with 10% fetal bovine serum (FBS, Gibco), and 1% v/v penicillin-streptomycin (pen/strep, Lonza). The cells are placed in a humid environment at 37°C with 5% carbon dioxide atmosphere. The cells are seeded into a 12 well-plate at a density of 2500 cells cm^{-2} and incubated for 24 hours to promote cell adherence. For days 1, 3, and 7 of cell culture, cell viability is assessed by using a live/dead assay (Thermofisher, USA). The cells are rinsed with phosphate-buffered saline (PBS) and stained with the live/dead reagent for a 30-minute incubation. Fluorescence microscopy images of cells are captured in at least six different randomly chosen areas utilizing the Zeiss LSM 900 Airyscan 2 confocal fluorescence microscope (Zeiss, Germany). The metabolic activity is evaluated on days 1, 3, and 7 using the Reassuring assay (Biotium, USA). In brief, the constructs are submerged in DMEM culture media with 10% v/v reassuring reagent and incubated for an hour at 37°C. After incubation, 100 µL of media is transferred to a 96-well plate, and

fluorescence is measured on a microplate reader at 530/571 nm excitation/emission wavelengths. Fluorescence readings are then normalized against a control well with a medium in the absence of biological samples.

Dynamic pH Monitoring: The pH sensor is secured at the center of a petri dish and linked to a potentiostat for measuring the open circuit potential. A GelMA (2.5% weight ratio) hydrogel film is formed by applying 16 μL of the precursor GelMA solution and curing it under UV light at a wavelength of 395 nm for 15 seconds. The GelMA hydrogel is then immersed in a pH 7.0 solution. Once the GelMA hydrogel is cured, 200 μL of a solution mixed with FBS and PBS at a 1:1 ratio (pH = 4) is applied to the opposite side of the hydrogel film using a micropipette.

Institutional Review Board Approval: The conducted human subject experiments were performed in compliance with the protocols. Exempt Self-Determination Tool was provided by the Institutional Review Board, Human Research Protections at the University of California, Irvine. All subjects gave written informed consent before participation in the study.

Chapter 4

Summary

In this study, we have tackled the challenges associated with wearable electronics fabrication by harnessing the capabilities of 3D printing. By leveraging this cutting-edge technology, we have overcome various hurdles and reaped the benefits it offers, including improved efficiency, cost-effectiveness, and simplicity compared to traditional micro/nanofabrication processes. Our research has resulted in the development of innovative wearable sensors capable of detecting multiple physiological signals with exceptional sensitivity.

In chapter 2, we introduce a flexible wearable pressure sensor fabricated using a novel approach called multi-material and multilayer 3D printing using nanocomposites. The sensor demonstrated high sensitivity, compressibility, and low detection thresholds. The fabrication process eliminated the need for cleanrooms, reducing costs and expediting production. The multilayer 3D-printed sensors exhibited excellent mechanical tolerance, high sensitivity (0.512 kPa^{-1}), rapid response time (94.6 ms), and a low detection limit (<0.009 kPa). The device holds potential for real-time health monitoring, robotics tactile sensing, and human-machine interfaces, showcasing the capabilities of this innovative wearable pressure sensor.

In Chapter 3, we developed a wireless, battery-free, and flexible wearable pH sensing system called W2BF3D. It integrated a disposable pH sensor and a reusable NFC readout system for real-time pH monitoring from sweat. The pH sensor and NFC circuit were

fabricated on flexible substrates, ensuring mechanical stability and flexibility. Utilizing a direct ink writing technique with a 3D printer, we successfully fabricated the components. The W2BF3D wearable pH sensor exhibited exceptional sensitivity, repeatability, and reproducibility across various pH ranges. It passed bending tests, demonstrating mechanical durability. Compared to previous sensors, our pH sensor showed high sensitivity (~ -29.45 mV/pH) and a strong correlation coefficient (0.999). In biocompatibility and validation tests, the W2BF3D wearable pH sensor displayed excellent performance, with 90% cell survivability and successful wireless measurement of pH values in artificial and actual sweat. Overall, our W2BF3D wearable pH sensing system provides an accurate, wireless, and non-invasive solution for real-time human healthcare monitoring, offering simplicity, efficiency, and cost-effectiveness. It has promising applications in personalized healthcare and can greatly improve personal healthcare monitoring.

References:

[1] S.-Z. Guo, K. Qiu, F. Meng, S. H. Park, and M. C. McAlpine, '3D Printed Stretchable Tactile Sensors', *Advanced Materials*, vol. 29, no. 27, p. 1701218, 2017.

[2] S. Zhang *et al.*, 'A wearable battery-free wireless and skin-interfaced microfluidics integrated electrochemical sensing patch for on-site biomarkers monitoring in human perspiration', *Biosens Bioelectron*, vol. 175, p. 112844, 2021.

[3] R. Rahimi *et al.*, 'A low-cost flexible pH sensor array for wound assessment', *Sens Actuators B Chem*, vol. 229, pp. 609–617, 2016.

[4] O. Atalay, A. Atalay, J. Gafford, H. Wang, R. Wood, and C. Walsh, 'A Highly Stretchable Capacitive-Based Strain Sensor Based on Metal Deposition and Laser Rastering', *Adv Mater Technol*, vol. 2, no. 9, p. 1700081, 2017.

[5] Y. Gao *et al.*, '3D-Printed Coaxial Fibers for Integrated Wearable Sensor Skin', *Adv Mater Technol*, vol. 4, no. 10, p. 1900504, 2019.

[6] S. NajafiKhoshnoo *et al.*, 'A 3D Nanomaterials-Printed Wearable, Battery-Free, Biocompatible, Flexible, and Wireless pH Sensor System for Real-Time Health Monitoring', *Adv Mater Technol*, p. 2201655, 2023.

[7] B. C.-K. Tee, A. Chortos, R. R. Dunn, G. Schwartz, E. Eason, and Z. Bao, 'Tunable Flexible Pressure Sensors using Microstructured Elastomer Geometries for Intuitive Electronics', *Adv Funct Mater*, vol. 24, no. 34, pp. 5427–5434, 2014.

[8] J. F. Fieselmann, M. S. Hendryx, C. M. Helms, and D. S. Wakefield, 'Respiratory rate predicts cardiopulmonary arrest for internal medicine inpatients', *J Gen Intern Med*, vol. 8, no. 7, pp. 354–360, 1993.

[9] M. Cretikos *et al.*, 'The objective medical emergency team activation criteria: a case–

control study', *Resuscitation*, vol. 73, no. 1, pp. 62–72, 2007.

[10] J. Yang *et al.*, 'Flexible, Tunable, and Ultrasensitive Capacitive Pressure Sensor with Microconformal Graphene Electrodes', *ACS Appl Mater Interfaces*, vol. 11, no. 16, pp. 14997–15006, Apr. 2019.

[11] D. J. Miller *et al.*, 'Analyzing changes in respiratory rate to predict the risk of COVID-19 infection', *PLoS One*, vol. 15, no. 12, p. e0243693, 2020.

[12] Q. Yi *et al.*, 'All-3D-Printed, Flexible, and Hybrid Wearable Bioelectronic Tactile Sensors Using Biocompatible Nanocomposites for Health Monitoring', *Adv Mater Technol*, vol. 7, no. 5, p. 2101034, 2022.

[13] J. Qiu *et al.*, 'Rapid-Response, Low Detection Limit, and High-Sensitivity Capacitive Flexible Tactile Sensor Based on Three-Dimensional Porous Dielectric Layer for Wearable Electronic Skin', *ACS Appl Mater Interfaces*, vol. 11, no. 43, pp. 40716–40725, Oct. 2019.

[14] H. Yamazaki, Y. Hayashi, K. Masunishi, D. Ono, and T. Ikehashi, 'A review of capacitive MEMS hydrogen sensor using Pd-based metallic glass with fast response and low power consumption', *Electronics and Communications in Japan*, vol. 102, no. 3, pp. 70–77, 2019.

[15] S. R. A. Ruth, L. Beker, H. Tran, V. R. Feig, N. Matsuhisa, and Z. Bao, 'Rational Design of Capacitive Pressure Sensors Based on Pyramidal Microstructures for Specialized Monitoring of Biosignals', *Adv Funct Mater*, vol. 30, no. 29, p. 1903100, 2020.

[16] Z. He *et al.*, 'Capacitive Pressure Sensor with High Sensitivity and Fast Response to Dynamic Interaction Based on Graphene and Porous Nylon Networks', *ACS Appl Mater Interfaces*, vol. 10, no. 15, pp. 12816–12823, Apr. 2018.

[17] R. Mazrouei, V. Velasco, and R. Esfandyarpour, '3D-bioprinted all-inclusive bioanalytical platforms for cell studies', *Sci Rep*, vol. 10, no. 1, p. 14669, 2020.

[18] M. O. F. Emon, F. Alkadi, D. G. Philip, D.-H. Kim, K.-C. Lee, and J.-W. Choi, 'Multi-material 3D printing of a soft pressure sensor', *Addit Manuf*, vol. 28, pp. 629–638, 2019.

[19] Z. Tang, S. Jia, C. Zhou, and B. Li, '3D Printing of Highly Sensitive and Large-Measurement-Range Flexible Pressure Sensors with a Positive Piezoresistive Effect', *ACS Appl Mater Interfaces*, vol. 12, no. 25, pp. 28669–28680, Jun. 2020.

[20] T. Xia *et al.*, 'Ultrahigh Sensitivity Flexible Pressure Sensors Based on 3D-Printed Hollow Microstructures for Electronic Skins', *Adv Mater Technol*, vol. 6, no. 3, p. 2000984, 2021.

[21] Y. Gao, C. Lu, Y. Guohui, J. Sha, J. Tan, and F. Xuan, 'Laser micro-structured pressure sensor with modulated sensitivity for electronic skins', *Nanotechnology*, vol. 30, no. 32, p. 325502, May 2019.

[22] S. Peng, P. Blanloeuil, S. Wu, and C. H. Wang, 'Rational Design of Ultrasensitive Pressure Sensors by Tailoring Microscopic Features', *Adv Mater Interfaces*, vol. 5, no. 18, p. 1800403, 2018.

[23] G. Yue, X. Ma, W. Zhang, F. Li, J. Wu, and G. Li, 'A highly efficient flexible dye-sensitized solar cell based on nickel sulfide/platinum/titanium counter electrode', *Nanoscale Res Lett*, vol. 10, no. 1, p. 1, 2015.

[24] L. J. Currano, F. C. Sage, M. Hagedon, L. Hamilton, J. Patrone, and K. Gerasopoulos, 'Wearable sensor system for detection of lactate in sweat', *Sci Rep*, vol. 8, no. 1, p. 15890, 2018.

[25] H. Park, W. Park, and C. H. Lee, 'Electrochemically active materials and wearable

biosensors for the in situ analysis of body fluids for human healthcare', *NPG Asia Mater*, vol. 13, no. 1, p. 23, 2021.

[26] S. Nakata, M. Shiomi, Y. Fujita, T. Arie, S. Akita, and K. Takei, 'A wearable pH sensor with high sensitivity based on a flexible charge-coupled device', *Nat Electron*, vol. 1, no. 11, pp. 596–603, 2018.

[27] M. M. Chaumeil *et al.*, 'pH as a biomarker of neurodegeneration in Huntington's disease: a translational rodent-human MRS study', *Journal of cerebral blood flow & metabolism*, vol. 32, no. 5, pp. 771–779, 2012.

[28] M. Chung, G. Fortunato, and N. Radacsi, 'Wearable flexible sweat sensors for healthcare monitoring: a review', *J R Soc Interface*, vol. 16, no. 159, p. 20190217, 2019.

[29] S. L. Percival, S. McCarty, J. A. Hunt, and E. J. Woods, 'The effects of pH on wound healing, biofilms, and antimicrobial efficacy', *Wound repair and regeneration*, vol. 22, no. 2, pp. 174–186, 2014.

[30] T. R. Dargaville, B. L. Farrugia, J. A. Broadbent, S. Pace, Z. Upton, and N. H. Voelcker, 'Sensors and imaging for wound healing: a review', *Biosens Bioelectron*, vol. 41, pp. 30–42, 2013.

[31] P. Escobedo *et al.*, 'Wireless wearable wristband for continuous sweat pH monitoring', *Sens Actuators B Chem*, vol. 327, p. 128948, 2021.

[32] E. Skrzydlewska, M. Sulkowska, M. Koda, and S. Sulkowski, 'Proteolytic-antiproteolytic balance and its regulation in carcinogenesis', *World journal of gastroenterology: WJG*, vol. 11, no. 9, p. 1251, 2005.

[33] J. J. Abbas, B. Smith, M. Poluta, and A. Velazquez-Berumen, 'Improving health-care delivery in low-resource settings with nanotechnology: Challenges in multiple

dimensions', *Nanobiomedicine (Rij)*, vol. 4, p. 1849543517701158, 2017.

[34] M. P. Browne, E. Redondo, and M. Pumera, '3D Printing for Electrochemical Energy Applications', *Chem Rev*, vol. 120, no. 5, pp. 2783–2810, Mar. 2020.

[35] M. P. Browne, F. Novotný, Z. Sofer, and M. Pumera, '3D Printed Graphene Electrodes' Electrochemical Activation', *ACS Appl Mater Interfaces*, vol. 10, no. 46, pp. 40294–40301, Nov. 2018.

[36] T. Chu, S. Park, and K. Fu, '3D printing-enabled advanced electrode architecture design', *Carbon Energy*, vol. 3, no. 3. John Wiley and Sons Inc, pp. 424–439, Jul. 01, 2021.

[37] Y. Xu *et al.*, 'Multiscale porous elastomer substrates for multifunctional on-skin electronics with passive-cooling capabilities', *Proceedings of the National Academy of Sciences*, vol. 117, no. 1, pp. 205–213, 2020.

[38] J.-C. Chiang and A. G. MacDiarmid, '"Polyaniline": Protonic acid doping of the emeraldine form to the metallic regime', *Synth Met*, vol. 13, no. 1, pp. 193–205, 1986.

[39] Y. Li, Y. Mao, C. Xiao, X. Xu, and X. Li, 'Flexible pH sensor based on a conductive PANI membrane for pH monitoring', *RSC Adv.*, vol. 10, no. 1, pp. 21–28, 2020.

[40] R. Rahimi *et al.*, 'Laser-enabled fabrication of flexible and transparent pH sensor with near-field communication for in-situ monitoring of wound infection', *Sens Actuators B Chem*, vol. 267, pp. 198–207, 2018.

[41] D. Maji, D. Das, J. Wala, and S. Das, 'Buckling assisted and lithographically micropatterned fully flexible sensors for conformal integration applications', *Sci Rep*, vol. 5, no. 1, p. 17776, 2015.

[42] P. Humpolicek, V. Kasparkova, P. Saha, and J. Stejskal, 'Biocompatibility of polyaniline',

Synth Met, vol. 162, no. 7, pp. 722–727, 2012.

[43] K. Unger, F. Greco, and A. M. Coclite, 'Temporary Tattoo pH Sensor with pH-Responsive Hydrogel via Initiated Chemical Vapor Deposition', *Adv Mater Technol*, vol. 7, no. 5, p. 2100717, 2022.

[44] Y. Song *et al.*, 'Wireless battery-free wearable sweat sensor powered by human motion', *Sci Adv*, vol. 6, no. 40, p. eaay9842, 2020.

[45] A. N. Andriianova, Y. N. Biglova, and A. G. Mustafin, 'Effect of structural factors on the physicochemical properties of functionalized polyanilines', *RSC Adv.*, vol. 10, no. 13, pp. 7468–7491, 2020.